FUNCTIONALIZED REDUCED GRAPHENE OXIDE VIA CLICK CHEMISTRY AS ANTIWEAR ADDITIVES FOR LUBE OIL

NADIA BINTI JAMAL

INSTITUTE OF GRADUATE STUDIES
UNIVERSITY OF MALAYA
KUALA LUMPUR

2017

FUNCTIONALIZED REDUCE GRAPHENE OXIDE VIA CLICK CHEMISTRY AS ANTIWARE ADDITIVES FOR LUBE OIL

NADIA BINTI JAMAL

DISSERTATION SUBMITTED IN FULFILMENT OF THE REQUIREMENTS FOR THE DEGREE OF MASTERS OF PHILOSOPHY

INSTITUTE OF GRADUATE STUDIES
UNIVERSITY OF MALAYA
KUALA LUMPUR

2017

UNIVERSITY OF MALAYA

ORIGINAL LITERARY WORK DECLARATION

Name of Candidate: Nadia Binti Jamal (I.C/Passport No: [redacted])

Matric No: HGA 140020

Name of Degree: Masters of Philosophy

Title of Dissertation ("this Work"): Functionalized Reduced Graphene Oxide via Click Chemistry as Antiwear Additives for Lube Oil

Field of Study: Chemistry (Nanotechnology)

I do solemnly and sincerely declare that:

(1) I am the sole author/writer of this Work;
(2) This Work is original;
(3) Any use of any work in which copyright exists was done by way of fair dealing and for permitted purposes and any excerpt or extract from, or reference to or reproduction of any copyright work has been disclosed expressly and sufficiently and the title of the Work and its authorship have been acknowledged in this Work;
(4) I do not have any actual knowledge nor do I ought reasonably to know that the making of this work constitutes an infringement of any copyright work;
(5) I hereby assign all and every rights in the copyright to this Work to the University of Malaya ("UM"), who henceforth shall be owner of the copyright in this Work and that any reproduction or use in any form or by any means whatsoever is prohibited without the written consent of UM having been first had and obtained;
(6) I am fully aware that if in the course of making this Work I have infringed any copyright whether intentionally or otherwise, I may be subject to legal action or any other action as may be determined by UM.

Candidate's Signature Date:

Subscribed and solemnly declared before,

Witness's Signature Date:

Name: Dr. Samira Bagheri

Designation: Senior Lecturer

FUNCTIONALIZED REDUCED GRAPHENE OXIDE VIA CLICK CHEMISTRY AS ANTIWEAR ADDITIVES FOR LUBE OIL

ABSTRACT

Outstanding properties of reduced graphene oxide (rGO) makes it suitable for application in many areas of developmental interests, especially functionalized lubricant additive. The procedure involved synthesizing graphene oxide (GO) via a modified Hummer's method, then functionalizing it with alkyne and azide compounds via click chemistry methodology over a copper sulphate catalyst. The physicochemical properties of the functional potential lubricant additives were evaluated using Fourier Transform Infrared Spectroscopy (FTIR), Raman Spectroscopy, X-ray Photoelectron Spectroscopy (XPS), X-ray Diffractometry (XRD), Thermal Gravimetric Analyser (TGA), and Field Emission Scanning Electron Microscopy (FESEM). The performance of the lubricant additive, density, viscosity, total acid number (TAN) and four-ball tests were used to determine the performance of the lubricant, while the Scanning Electron Microscope (SEM) were used to generate the image the worn surfaces post-friction test. This indicates the dispersibility and tribological properties of the F-rGO in base oil. Interestingly, the organic moiety in the functionalized rGO was shown to improve its flexibility and stability, while the rGO itself provides hardness. However, the dispersed F-rGO improved the tribological properties of the resulting lubricant, which reduces both the friction coefficient and wear by 36 % and 24 %, respectively. These values suggested that the improved friction and antiwear properties are due to the functionalized rGO and the thin laminated structure, which is duly confirmed by the XRD and FESEM, respectively. These features also induce low shear stress and prevent direct contact between the metal surfaces according to the friction and wear test.

Keywords: graphene oxide; click chemistry; antiwear additive; solid additive.

GRAFENA OKSIDA TERKURANG YANG DIUBAHSUAI MELALUI KLIK KIMIA SEBAGAI BAHAN TAMBAH ANTIHAUS UNTUK MINYAK PELINCIR

ABSTRAK

Grafena oksida terkurang (rGO) memiliki ciri-ciri yang sangat sesuai untuk proses penambahbaikan terutamanya sebagai bahan tambahan bagi minyak pelincir. Grafena oksida (GO) dalam kajian ini disediakan menerusi proses Hummer yang telah diubahsuai, kemudian bahan tersebut diubahsuai lagi dengan penambahan kumpulan alkina dan azida menerusi kaedah kimia klik dengan menggunakan tembaga sulfat sebagai pemangkin. Ciri-ciri fizikal dan kimia bahan tambah ini dianalisa menggunakan Spektroskopi Inframerah Transformasi Fourier (FTIR), Spektroskopi Raman, X-ray Fotoelaktron Spektroskopi (XPS), Pembelau X-ray (XRD), Thermal Gravimetric Analyser (TGA), dan Mikroskop Bidang Pelepasan Elektron (FESEM). Seterusnya prestasi bahan tambah ini dianalisa daripada aspek ketumpatan, kelikatan dan jumlah nombor asid. Ujian empat bola telah digunakan bagi menentukan prestasi bahan pelincir tersebut, manakala Mikroskop Pengibas Elektron (SEM) digunakan untuk pengimejan permukaan selepas analisa. Hal ini menjadi penanda aras bagi tahap penyebaran dan ciri-ciri tribologi bagi bahan tambahan tersebut. Penambahan kumpulan organik pada grafena oksida membawa penambahbaikan kepada fleksibiliti dan kestabilan pada bahan tersebut yang secara natural memberi keutuhan. Penambahan bahan ini membawa kepada pengurangan kepada pekali geseran sebanyak 36 % dan pengurangan tahap kehausan sebanyak 24 %. Pengurangan ini menjadi bukti bahawa bahan tambahan ini telah meningkatkan keupayaan bahan ini sebagai bahan antihaus. Bahan berstruktur berlamina seperti yang ditunjukkan dalam FESEM turut memberi pengurangan kepada tegasan ricih dan menghalang hubungan terus antara dua permukaan.

Kata kunci: Grafena oksida; klik kimia; bahan tambah antihaus; bahan tambah pepejal

ACKNOWLEDGEMENTS

Alhamdulillah, praises to Allah SWT for giving me the strength to endure all the challenges and complete this study within the time given. First and foremost, I would like to express my outmost gratitude to my super kind-hearted supervisors, Dr Samira Bagheri and the late Prof Sharifah Bee Abd Hamid for the useful comments, remarks, engagement, patience, persistence encouragement and invaluable assistance through the learning process of this study from the beginning till the end of this study. Thank you so much for your time and hard work to guide me through this project and I am really glad and proud to be under your supervision.

Special thanks also goes to the Ministry of Education Malaysia and University of Malaya for financial support through MyMaster15 as well as Catalysis Research Centre (NANOCAT), University of Malaya for laboratories and equipment facilities. A warmest thankful also intended to all science officers who got involved in this project whether directly or indirectly.

Love and thanks to my parents, brother and sisters for their love and constant supports. I thank them for simply being there and loving me with all their hearts. Not forgetting, my fellow course mates for their brilliant ideas, helping me putting pieces together as well as their guidance and moral support. Thank you for the bond of friendship and for making me stay in University of Malaya a bearable one with many unforgettable memories and experiences.

May Allah bless all of you. Thank you so much.

TABLE OF CONTENTS

LIST OF FIGURES

LIST OF TABLES

LIST OF SYMBOLS AND ABBREVIATIONS

ASTM	:	American Society for Testing and Materials
C	:	Carbon
C10	:	Ten carbon length
C12	:	Twelve carbon length
C6	:	Six carbon length
C8	:	Eight carbon length
CNTs	:	Carbon nanotubes
CoF	:	Coefficient of friction
CSt	:	Centistokes
CuAAC	:	Copper-Catalyzed Azide-Alkyne Cycloaddition
DFT	:	Density Functional Theory
DMF	:	Dimethyl formamide
EDX	:	Electron Dispersive X-ray
EP	:	Extreme pressure
F-rGO	:	Functionalized reduced graphene oxide
FTIR	:	Fourier Transform Infrared Spectroscopy
GO	:	Graphene oxide
H	:	Hydrogen
h-BN	:	Hexagonal boron nitride
HFRR	:	High Frequency Reciprocating Rig
KBR	:	Potassium bromide
MoS_2	:	Molybdenum disulphite
MWCNTs	:	Multi-walled carbon nanotubes
N	:	Nitrogen

O	:	Oxygen
PAO	:	Polyalphaolefins
rGO	:	Reduced graphene oxide
SEM	:	Scanning Electron Microscope
TAN	:	Total acid number
TCP	:	Tricresyl phosphate
TGA	:	Thermogravimetric Analyser
THF	:	Tetrahydrofuran
WSD	:	Wear scar diameter
wt. %	:	Weight fraction
XPS	:	X-ray Photoelectron Spectroscopy
XRD	:	X-ray Diffractometer
ZDDP	:	Zinc dithiophosphate

LIST OF APPENDICES

CHAPTER 1: INTRODUCTION

1.1 Research background

Mitigating the detrimental effect of frictional force upon two surfaces in motion with respect to one another with the aid of additives helps increase the lifespan of working tools and engineering machineries, as well as energy facilities. Many substances have evolved as suitable additives for controlling friction. Liquid lubricants, for instance, prevents sliding interfaces from severe damage by forming a boundary film with low shear and high durability (Espinosa et al., 2016; Fajardo et al., 2015; Raghunanan & Narine, 2016a, 2016b, 2016c). They limit wear due to the limited boundary surface thickness and sensitivity towards surrounding heat energy. A solid additive that could leverage the aforementioned lubricant challenge is molybdenum disulphide (MoS_2), which forms strong films on metallic surfaces and exhibit high lubricity and stability at a temperature of less than 400 ^oC in a dry and vacuum-type environment. However, MoS_2 loses its lubricity in oxygen or water environment (Huang et al., 2005; Rudnick, 2009; Sunqing et al., 1999; Xiaodong et al., 2007). Graphite self-lubricating and dry lubricating properties could be a better option due to its resistance to the detrimental effect of prolonged exposure to continuous temperatures of up to 450 ^oC while being exposed to oxidising agents. The advantage is that despite all this, graphite remains capable of providing effective lubrication. However, it suffers from degraded functionality in the event that its surroundings lack humidity (Rudnick, 2009). Another lubricant such as boron nitride is a ceramic, with robust tolerance against high temperatures of up to 1200 ^oC, even in an oxidizing atmosphere (Kimura et al., 1999). Antiwear additives such as Zinc dialkyldithiophosphate (ZDDP) is a valuable anti-oxidant and corrosion inhibitor. Unfortunately, at 130-170 ^oC, it decomposes, and discharges phosphorus, which is regarded as a poisonous substance (Kasrai et al., 1998; Unnikrishnan et al., 2002). Tricresyl phosphate (TCP), on the other hand, has an activation temperature that typically

exceeds 200 ºC, and it forms a chemical bond that acts as a lubricating film on the surfaces. However, it is a health hazard, and is known to induce depression and schizophrenia (Godfrey, 1965; Lu et al., 2009).

Against the preceding background and the disadvantages of the antiwear additives, we developed an innovative antiwear additive via the click chemistry functionalisation of reduced graphene oxide. This antiwear material possesses friction and antiwear properties that are unique. Its inertness, high level of mechanical strength, and ease of shearing for impressive tribological behaviour are some of its properties that warrant applications (Berman, Erdemir, & Sumant, 2014; Dreyer, Park, Bielawski, & Ruoff, 2010; Stankovich et al., 2007). When coupled with the intercalating attributes of reduced graphene, we developed this material with the intention to minimise its tendency to precipitate, which occurs when its mixed with water or any other organic solvents. Hitherto, reduced graphene has found its place as an oil additive, usually with the intention of improving lubricity and reducing wear (Lin et al., 2011). Evidence in previous tribological studies show that reduced graphene has high self-lubricating potential that reduces friction and wear on surfaces (Li et al., 2005; Shioyama & Akita, 2003), which is in line with that of the edge plane of reduced graphene oxide in this study, where it was functionalized with a highly electron-rich group to boost its tribological properties. We focussed on producing a highly dispersed functionalized reduced graphene as a promising additive that enables low resistance in sheared contact by means of weak van der Waals interaction, thus bringing about a significant reduction of friction and wear between sliding surfaces.

1.2 Statement of the problem

In any form of mechanical construct, reducing the wear effect from friction remains a challenge, even with our current access to modern technology, especially in the case of extreme conditions (Berman et al., 2013). Henceforth, continuous studies on various new materials for coating and lubrication that can potentially reduce friction and wear have been conducted. Unique physicochemical properties of graphene makes it a potent material for many tribological applications, where negating the effect of friction and wear is paramount at different length scales (Berman et al., 2014). However, challenges include dealing with graphene's inherent tendency to agglomerate due to its strong intermolecular interaction, and also its lack of solubility in base oil, which limits its effectiveness as an additive. If not reduced or effectively controlled, high levels of friction will significantly increase the level of losses due to wear, hence shortening the instrument's life span and reliability.

1.3 Justification for the study

Challenges include graphene's tendency to aggregate due to the strong intermolecular forces between the particles and its lack of solubility in base oil, which limits its effectiveness as an additive, both of which are the main focus of this work. By chemically introducing a new functional group onto the surface of graphene via click chemistry, the negative aspects of graphene as an additive can be reprimanded. Functionalisation of reduced graphene, specifically by click coupling, is able to tailor the properties to improve its dispersive capability in base oil, which enhances the tribological properties of oil. This is achieved by manipulating GO's surface to obtain functional groups that serve as precursors to anchor desirable molecules.

1.4 Aim and objective of the research

The main focus of this work is to determine the possible properties of functionalized graphene for application in lube oil.

Specific objectives of this research are as follows:

1. To synthesise functionalized rGO (F-rGO) via Click Chemistry (Cu-Catalyzed Azide-Alkyne Cycloaddition) with various aliphatic chains for high dispersity in oil.
2. To determine and investigate the suitable type of F-rGO and its potential for use as an antiwear additive for lube oil.

1.5 Scope of the research

The scope of this study is to synthesise functionalized rGO with different alkyl chains and investigate its activity in base oil as an additive. The intention is to reduce the friction and wear between metal-to-metal contact, which is mainly used in tribological industries. The major theme of the present research is to synthesise antiwear additives that can be used in base oil at a much lower cost.

1.6 Outline of the dissertation

This dissertation is divided into five sections, organised in the following order:

Chapter 1

This chapter introduces the study and provide a detailed background to the work, along with the statement of research problem, justification for the study, the aim and objectives of the study, and the scope of the research.

Chapter 2

This chapter starts with a literature survey on previous studies, which is intended to provide an understanding of the knowledge and theories pertaining to tribology. The tribological properties of different types of solid additives and the various mechanisms that have been proposed to explain their tribological behaviours will also be discussed.

Chapter 3

This chapter will describe the synthesis procedure for the additives and the experimental techniques used to characterise the additives and investigate the friction and wear behaviours of the additives in base oil as alongside it's working mechanism. The testing materials used in this study will be introduced in this chapter.

Chapter 4

This chapter will present the experimental results and observations obtained from tribological tests using functionalized reduced GO as an additive in base oil. The results from both the additives' characterisation and performance test will be presented. The friction and wear reduction mechanisms of F-rGO will be discussed as well.

Chapter 5

This chapter summarises the main findings from the overall study, as well as suggestions for future research in this area.

CHAPTER 2: LITERATURE REVIEW

2.1 Introduction to Tribology

Tribology is defined as the science and engineering of interacting surfaces in relative motion, encompassing fields of friction, lubrication, and interactions between solids, liquids, and gases (Handbook & Friction, 1992).

2.1.1 Friction

Amontons' empirical laws of friction are comprised of four theorems. The first one being that the maximum tangential force is proportional to the normal force when a static body is subjected to an increasing tangential load. The second law describes the tangential friction force, which is described to be proportionate to the perpendicular force during sliding. The third and fourth laws describe the independence of the friction force to both variables of apparent contact and sliding speed. These laws have been proven to be applicable in a variety of material and tribosystems, with observed limitations when polymers are involved (Sakamoto et al., 1985). Derivation from the second law resulted in the following equation:

$$F = \mu \bullet P \qquad \textbf{(Equation 2.1)}$$

where P is the normal load, F is the tangential force, while μ is the coefficient of friction. In many ways, frictional force is necessary in our daily life, in fact, linear motion may not be entirely possible without the existence of such force. Conversely, a motion will not be able to be stopped without the existence of frictional force, which is how brakes actually work in motor vehicles. In terms of gears and machinations, force is detrimental due to surface wear, which reduces their efficiency. These laws of frictional force govern our understanding of the mechanics of frictional force, which includes tribology.

2.1.2 Mechanism of Wear

The mechanical action of opposing surfaces will eventually result in the removal and/or deformation of material from the surfaces, which is commonly known as wear. This is undesired, especially in machineries, as it decreases efficiency (Suh, 1973). Wear can be further categorised into four types, namely abrasive, adhesive, fatigue, and corrosive, and each are differentiated by its material removal mechanisms from the surface.

2.1.2.1 Abrasive wear

Abrasive wear is present between a rough and soft surface, where the asperity from one surface, usually the rougher one, penetrates the other, resulting in material removal (ASTM, 2013). The debris from the microcutting mechanism will be dislodged from its original surface, producing ridges (Khruschov, 1974). Abrasive wear can be further divided into two sub-categories, as shown in Figure 2.1. The first is a two-body mode, where the abrasion of a soft surface takes place due to the penetration by a hard counterpart, thus producing debris. The second mode is the three-body mode, where the debris are free to slide along a surface, or in other cases, roll off of it.

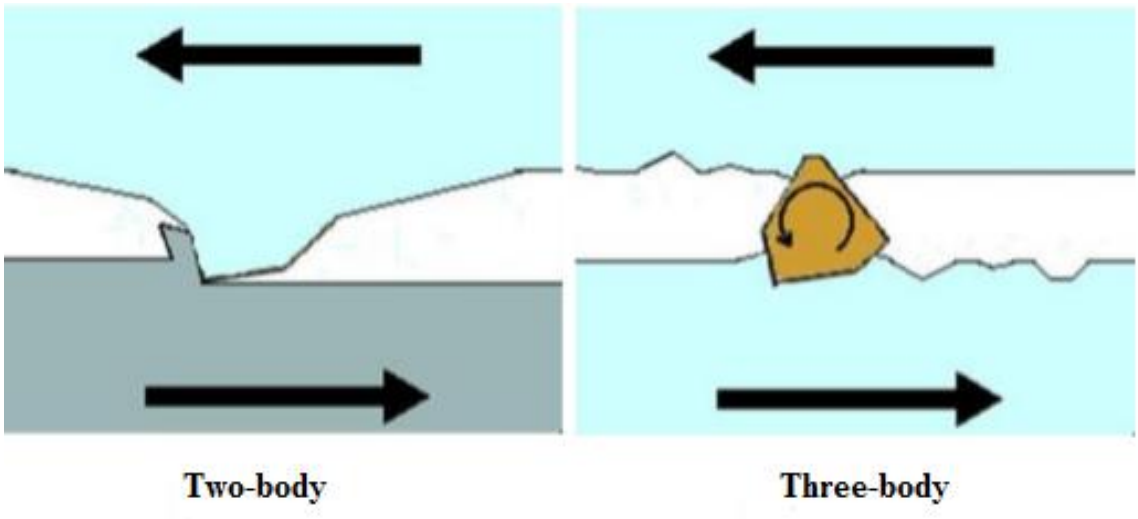

Figure 2.1: Schematic view of abrasive wear (Khruschov, 1974)

2.1.2.2 Adhesive wear

The sliding of two surfaces, especially when exposed to harsh contact, leave them vulnerable to adhesive wear. This form of wear involves the detachment of the material from one of the surfaces in contact, as illustrated in Figure 2.2. The material will likely be transferred to the other surface, which would result in zero net loss of material were it not for the fact that the transferred material will be held very loosely by the surface. The process takes place at a microscopic scale, and the effect will only be more prominent with time. Such effects include torn surface with grooves and transferred ridges of material (Kato, 1992). Oxidation films and lubricants are often applied between these surfaces to reduce the adhesion forces that contribute to adhesive wear. However, wearing of the surfaces will still take place, especially in the presence of high load and shear rate. Hence, additives that can interact rapidly with the surfaces are often added to the lubricant to form a protective film to reduce the detrimental effect of adhesive wear (Rabinowicz, 1965).

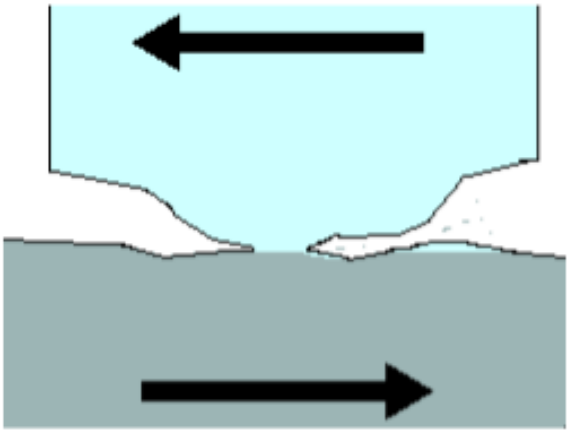

Figure 2.2: Schematic of Adhesive wear (Rabinowicz, 1965)

2.1.2.3 Corrosive wear

A product of chemical reaction can be continuously removed when the reaction takes place on two sliding surfaces. This repeated removal in the event of chemical reactions process is known as corrosive wear, as it takes place in a corrosive surrounding. It is relatively easier to chafe the product of the reaction compared to the starting material, making this a continuous process, at least up till the point the substrate runs out, or is removed from the corrosive environment. It should be pointed out that the wear rate is proportional to the rate of the chemical reaction, which represents its main mechanism.

2.1.2.4 Fatigue wear

A material is in a rolling/sliding motion will generate local stress. Repeated contacts between the aforementioned material with asperities will result in fatigue wear (Suh, 1973). This form of wear usually initiates other form of wears (abrasive and adhesive). As shown in Figure 2.3, the top material will be removed, and catastrophic wear will take place when these cracks reach a critical size (Suh, 1973). Within a system, the dominant wear mode may not be constant. There are many factors influencing the transition of wear modes, such as changes of contact geometry, by altering the properties of the rubbing surfaces using lubricant additives (J. Xu et al., 1997) .

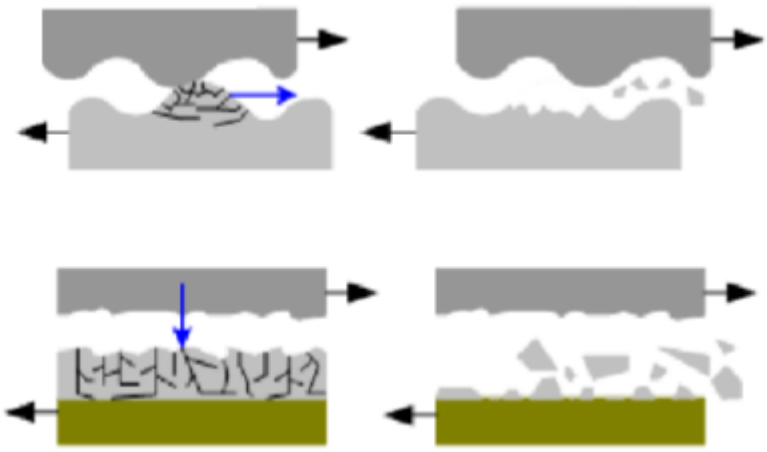

Figure 2.3: Schematic of Fatigue wear (Rabinowicz, 1965)

2.1.3 Lubrication

Introducing a film of lubricant between two in-contact surfaces in motion is often employed to reduce wear of mechanical parts due to friction. The lubricant may be oil-based or in some cases water-based. This thin layer is now vital towards ensuring the longevity of the mechanical parts. In case of lubricated systems, the Stribeck curve shown in Figure 2.4 describes the dependence of the friction coefficient on the dynamic viscosity, η, the speed, ν, and the normal load, L. There are three regime scan that are apparent, which are hydrodynamic lubrication, mixed lubrication, and boundary lubrication.

In the case of a hydrodynamic lubrication system, the adjacent surfaces are totally separated by a thick lubricant film (1-1000 μm) preventing the sliding on surfaces, while the load is supported by the lubricant film. The low coefficient of friction arises from the shear forces in the viscous lubricant. The friction coefficient is calculated from Reynold's equation, where the friction coefficient is directly proportional to the load, while the viscosity is inversely proportional to the sliding speed.

The mixed lubrication regime is where the lubricant films are thin (0.01-1 m) and some asperities from the two surfaces are in contact. The load along the asperities in contact are carried supported by the lubricant film. The two surfaces are separated from each other partly by hydrodynamic forces and partly by thin layers of lubricant adhering to the surface's contours. It is an intermediate state where the strict laws of hydrodynamic lubrication are no longer fully applicable.

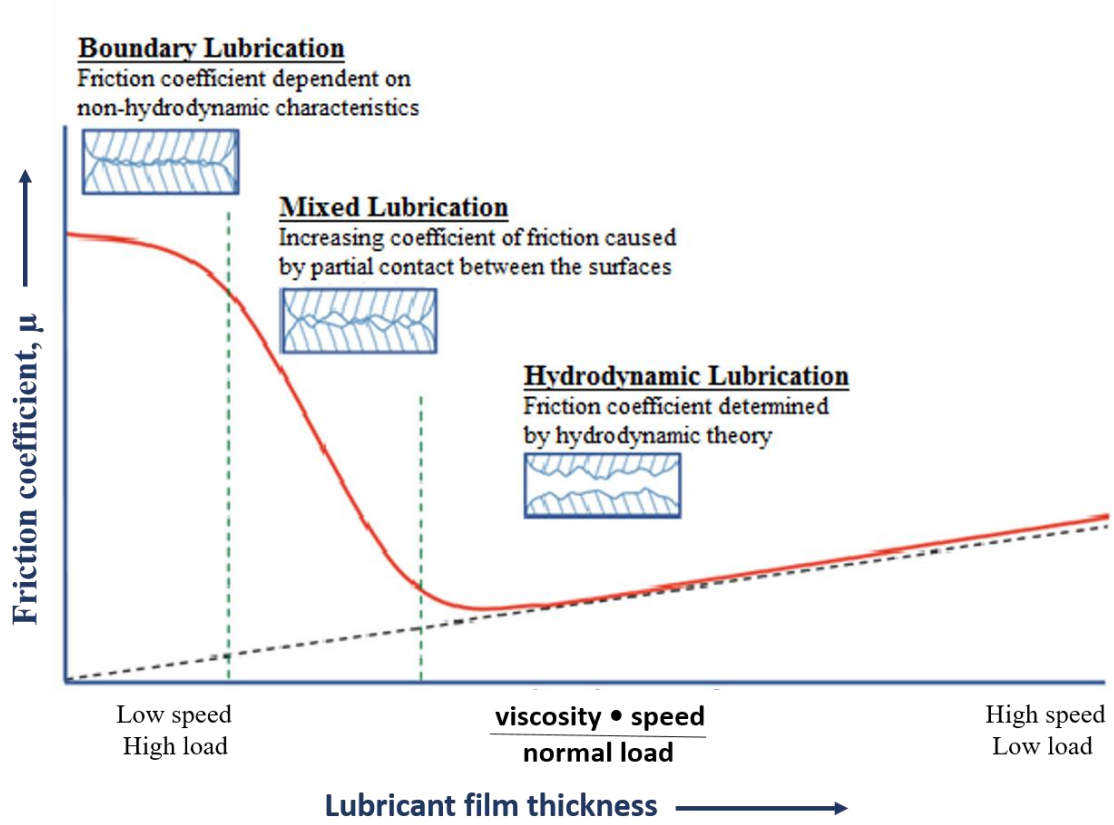

Figure 2.4: Stribeck curve, dependence of the friction coefficient on viscosity, speed and load for a lubricated sliding system (Sakamoto et al., 1985)

Typically, lubricating films have an average boundary thickness of 1-100 nm. This range is still lower than the composite thickness of surface asperities and roughness that are in contact during motion. Boundary lubrication negates the contact between asperities from the two surfaces that are in motion relative to one another. Collision between the two surfaces often results in deformation and fractures that were formed locally on the surfaces. Local conditions at the boundary lubrication causes induction of direct chemical reaction between the molecules of the lubricant and the material of the surfaces involved. This is typical when considering the overall effect of flash temperature and abraded surfaces. The chemical reactions thus increase the friction coefficients (Suarez et al., 2010).

2.2 Lubricants

Lubricants are formulated products composed of a base oil (or base stock), and various specialty additives designed for specific performance needs. They reduce friction and wear, keep the components cool, and remove wear debris, while base oil functions as a solvent for the additives as it controls the bulk and surface properties. Additive levels in lubricants range from 1 - 25 wt.%, based on it intended applications (Jianqiang et al., 2005).

2.2.1 Base oil

There are a few criteria when discussing a base oil as a foundation for lubricating mixture. First, in order to maintain the lubrication film, the oil must be of a suitable viscosity with respect to varying operating parameters. This ensures fluidity of the oil and its ability to remove heat while congruently avoiding power loss. In this aspect, the thermal stability of the oil is crucial. Simultaneously, the oil should also be stable against oxidation, of low volatility, and capable of negating frictional forces that consequently reduces wear. A good base oil is thos(Berman et al., 2014)e that can dissolve additives while remaining inert vis-à-vis materials it comes into contact with.

2.2.1.1 Mineral Oil

Mineral oils make up the base stock in most formulation of lubricants. Straight and/or branched carbon chains, made up of 20 - 40 carbon atoms in each molecule, are the main composition of mineral oils. At times, the mineral oil may contain aromatic or aliphatic rings. Sulphur, nitrogen, or oxygen found in a variety hydrocarbon structures, complete the remainder of the oil's composition. The heteroatoms influence the base oil's stability and can affect the lubricating properties, as they may interfere with the lubricant additives. To distinguish between refined and crude oil, one may study the oil's chemical form, viscosity, and the amount of sulphur. Further categorisation of mineral oil comes in three

forms. Paraffinic oil is made up of straight or branched chain hydrocarbons, while naphthenic oil is composed mainly of hydrocarbons containing cyclical carbon based molecules with no saturated bonds. Finally, benzene type compounds generally make up aromatic oil.

The origin of any crude oil is the main determinant of the sulphur content in the oil, ranging from 0 – 8 wt. %. Sulphur, in moderate amounts in the oil, is desirable as it improves resistance against oxidation and lubricating capabilities, both of which reduces wear (J. Zhang et al., 1998). The viscosity of mineral oils is a function of the level of oil refinement.

2.2.1.2 Synthetic Oil

The structure of synthetic oils, such as carbon chain and functional groups, can be designed for specific properties. Synthetic oils are used for more demanding applications, such as insulation, or thermal and chemical resistant lubricants (Boshui et al., 1996), which makes them more expensive.

(a) ***Polyalphaolefins***

Polyalphaolefins are unsaturated carbon chain with an unsaturated carbon at the end. The unsaturated carbons are the primary active site that initiates oligomerization to form lubricants. Among its most important features are high viscosity index of 120 - 170, low volatility, and stability against oxidative reactions. However, the lack of unsaturated carbons in the form of functional groups, such as double bonds and aromatic containing structures, render their solubility in additives quite low.

(b) ***Esters***

Esters are manufactured by reacting any form of alcohol with fatty acids. They are classified based on the number of ester groups substituted in the fatty acid. For example,

an ester with single ester group is known as monoester. In term of viscosity, monoesters tend to have lower viscosities compared to diesters or polyesters. Diesters have a good viscosity index and good low temperature properties, but fairly low viscosities (7 - 46 cSt). The main distinguishing feature of a polyester compared to diesters is that the viscosity lies in a wider range depending on factors such as the degree of esterification.

2.2.2 Lubricant Additive

Additives enhances the performance of lubricants in a variety of applications. These additives can be further classified into those that are active or inert to further chemical reactions. The former interface chemically with metals and polar oxidation and degradation products, thus forming protective layers and making them innocuous. These chemicals are often applied to improve the characteristics of the lubricant, such as dispersants improving the dispersability and oxidative inhibitors prolong service life of the lubricant. Chemically inert additives enhance the vital physical properties, without which the performance of the lubricant has been shown to plummet significantly, such as in the case of emulsifiers and demulsifiers (Jianqiang et al., 2005). Most lubricant additives, except perhaps some viscosity improvers and pour-point depressants, consist of an oleophilic hydrocarbon group and a hetero atom (N, O, S, and P)-based polar functional group as illustrated in Figure 2.5. The hydrocarbon group must have a sufficient length of chain carbon to achieve the required solubility characteristics of the additive. The additives that require greater solubility in oil (dispersants, detergents, and viscosity improvers) usually contain large hydrocarbon groups. Those that require either lower solubility or greater surface activity (foam inhibitors and extreme-pressure) contain small hydrocarbon groups. The performance of the additive is strongly dependent on a proper balance of polar and non-polar characteristics (Jianqiang et al., 2005).

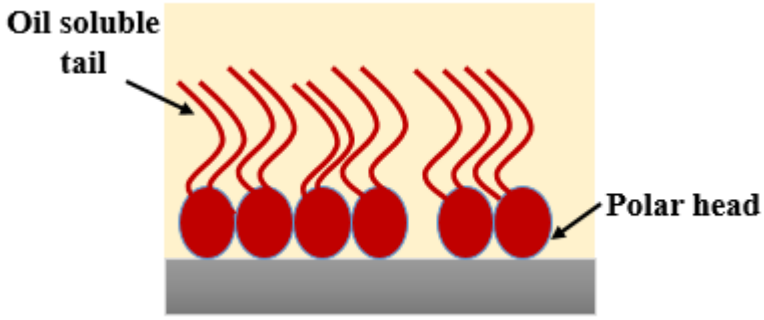

Figure 2.5: Additive structure scheme

To modify the properties of the lubricant, it needs many types of additives. Viscosity modifiers, such as polymers, are often introduced to the fray with the intention of positively altering the viscosity of the oil and improve the flow properties in cold lubricants by decreasing the pour-point, which also decreases the crystallisation temperature. Corrosion inhibitors protect the surfaces from harmful species that react detrimentally with the aforementioned surfaces in the solution by adsorbing onto the surface and sterically hindering interactions with the reactive species' surface. Detergents and dispersants, e.g. amphiphiles, are attached to oxidative or degradation products or dirt particles, which results in oil-soluble species, preventing deposition on the surface. The oil might oxidise via thermally activated dissociation of a hydrogen atom from the hydrocarbon chain, or be induced by the presence of a nascent iron. The resulting radical carbon chain reacts with dissolved oxygen to form peroxides, which in turn induce further radical formation and oxidation. This leads to a higher acidity and lowered viscosity of the lubricant. To prevent these effects, antioxidants such as metal deactivators, radical inhibitors, or peroxide decomposers are added. Silicone polymers are added in very low amounts to minimise foaming by decreasing surface tension.

The modifiers that combats frictional force and wear are vital additives when accounting for economical and performance issues. In the boundary lubrication regime, the surface asperities are in direct contact, promoting high level friction and increased rate of wearing. This direct exposure of asperities on the surfaces have to be reduced,

which introduces a protective film on the surface. There are three types of additives: The friction modifiers, also called adsorption or boundary additives, are used to inhibit stick-slip via physical adsorption onto the surface, forming thin layers that prevent adhesion and microwelding. Usually amphiphiles with polar head groups, such as alcohols, esters, unsaturated and saturated acids bound on aliphatic chains are utilized. They adsorb onto the surface and prevent direct contact. Usually these additives only work at low loads and temperatures below 80 °C. At higher temperatures, the additives desorb upon thermal activation. Another group of friction modifiers is that of organomolybdenum compounds (e.g. molybdenum dithio-carbamates). The mixed and boundary lubrication regimes introduce antiwear additives that are able to interact with the surfaces involved to form a layer of protective film, which ensures that the sporadic asperity on the surfaces do not lead to severe damage from wear. These additives are phosphorus-based, with zinc dialkyl dithiophosphates (ZDDP) being the most commercially applied in engine systems, which forms one of the major sources of phosphorus and sulphur in engine oils. Other additives include tricresylphosphate (TCP) and other phosphate esters or phosphorotionates. Microwelding becomes prominent only under severe boundary lubrication conditions, such as in slowly moving and heavily loaded gears. The additives react with the surface to prevent this from occurring. These additives are sulphur-based, which includes dibenzylsulphide, phosphosulphurised isobutene, trichloroacetone or molybdenum disulphide (MoS_2), all of which are able to withstand extreme pressure.

2.3 A journey from GO to graphene

One of the earliest research leading up to the discovery of graphene was carried out in 1859, where it was first known as graphitic acid due to its insolubility in acidic and alkaline solutions, but it demonstrates high dispersability in aqueous solution. The core of the method is oxidising graphite in an acidic mixture of potassium chlorate and nitric

acid. Further characterisation reveals molecular information of the material, including its composition of mainly carbon, hydrogen, and oxygen, as yielding a molecular formula of $C_{2.19}H_{0.80}O_{1.00}$. The synthesized material laid the foundation for the modern synthesis of graphene (Brodie, 1859).

This idea was expanded by Staudenmaier in 1898, who used concentrated sulphuric and nitric acids with potassium chlorate to oxidise the graphite flakes. The gradual increase of potassium chloride in this method was designed to accelerate the rate of oxidation of graphite without having to repeat the same process reported by Brodie. As a result of this, the degree of oxidation of graphite became similar to Brodie's method, where the ratio of carbon to oxygen is almost equal, at 2:1. This method, despite being more practical, is inherently more dangerous. In 1958, Hummers and Offeman modified this method by developing a safe procedure for oxidising graphite flakes that took less than two hours. They treated graphite flakes with a water-free mixture of concentrated sulfuric acid (H_2SO_4), sodium nitrate ($NaNO_3$), and potassium permanganate ($KMnO_4$), resulting in the similar levels of oxidation (Hummers Jr & Offeman, 1958).

Since then, Hummers' method was used to produce GO, with slight modifications in order to avoid generating toxic gases and reduce processing time, which results in higher levels of oxidation. In 2010, Marcano *et al.* described an improved method of synthesising GO by excluding nitric acid, increasing the amount of $KMnO_4$, and performing the reaction in a 9:1 mixture of H_2SO_4/H_3PO_4. This procedure produced a large-scale hydrophilic GO, with fewer defects in the basal planes (Marcano et al., 2010). This process also did not generate toxic gases, and it improved the graphite oxidation efficiency, increasing its oxidation levels compared to Hummers' method.

Current researchers are more interested in producing graphene with the thinnest layer possible, where the carbon atoms were arranged in lattices patterned not unlike

honeycombs as shown in Figure 2.6. This is to further enhance the material's already remarkable physical and electrical properties for applications in various fields. Andre Geim and Konstantin Novoselov managed to produce graphene at millimetres via the micromechanical cleavage method, which involves the peeling of individual graphene layers from graphite synthesized from graphite flakes (Novoselov & Geim, 2007).

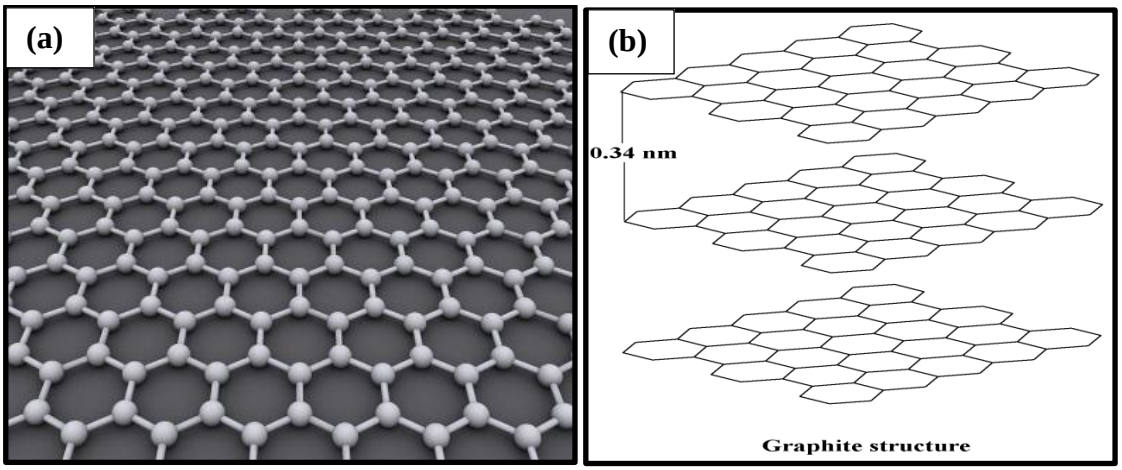

Figure 2.6: (a) One atom thick graphene in honeycomb lattice (b) The d-spacing of graphene (Novoselov & Geim, 2007)

Various methods have been employed to synthesise an isolated layer of graphene, such as chemical deposition (Bautista & Mendoza, 2011) and thermal reduction (Chen et al., 2010). The research trends then began to focuses on hybridisation of these isolated sheets of graphene with materials such as polymers (Carotenuto et al., 2015), metal (C. Xu et al., 2008) and metal oxides (Zou & Wang, 2011) to further enhance the base material's applicability, such as electron transportation and thermal conductivity.

To combat graphene's tendency to agglomerate irreversibly due to its hydrophobicity, the material's surface was functionalized. The simplest solution to agglomeration is functionalising graphene with hydrophilic groups, yielding nano-composite materials (Tantis et al., 2012). Overcoming the issue of hydrophobicity via surface functionalisation also prevents the reformation of graphite.

2.3.1 Properties of graphene

The building blocks of graphene are sp^2 carbon atoms arranged in honeycomb-like 2D lattices. Each individual carbon atoms form trigonal planar structures with their neighbours, with each atom having a delocalised π orbital as in Figure 2.7.

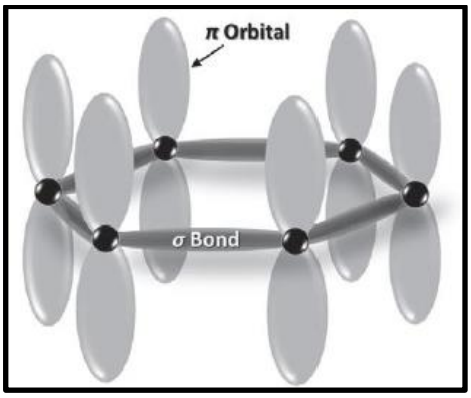

Figure 2.7: The sp^2 hybridize orbitals between carbon atoms and the π bonds (Novoselov & Geim, 2007)

The strength of the C-C bonds between the atoms contribute to graphene's mechanical strength, while the delocalised orbitals make it an excellent material for electronic applications with good electron transporting properties. As an added benefit, graphene possesses very high specific surface area and is an excellent thermal conductor.

2.3.2 Functionalized rGO

Reacting graphene with organic and inorganic molecules, or even modifying the surface of graphene oxide yield a functionalized form of rGO (Georgakilas et al., 2012). The general idea is reacting the functional groups on the surface of graphene oxide with compounds containing functional groups. These functional groups will then act as an anchor for further modification with other molecules. The resulting material have been shown to demonstrate improved dispersability in various solvents. These functionalized materials lay the foundation for further nucleation of nanoparticles, promoting uniform particle size and the dispersion of nanoparticles throughout the overall material (Marques et al., 2011).

2.3.3 Functionalized rGO as an additive

As discovered by Peng *et al.*, introducing diamond nanoparticles as an additive improves its ability to prevent friction, and interestingly, the improvement becomes increasingly prominent with decreasing particle sizes of the additive. Recently, GO was used in the same manner as diamond nanoparticles as additives. The unique advantage using GO is the customisability of the material due to presence of –OH and –COOH groups on its surface. These groups allow for the functionalisation of either long chain compounds, such as aliphatic amine or compounds containing more –OH and –COOH groups. The first of these aforementioned functionalisation enhances GO's dispersability in non-polar solvents, while the latter increases its polarity to prevent GO from undergoing chemical reactions, which also increases its stability (D. Peng et al., 2009).

The ability to functionalise an additive is particularly important when solid lubricants are involved. These lubricants include graphite and MoS_2 which are composed, at the molecular level, of flat sheets of molecules, or in some cases, merely atoms. The sheets make it easy for the material to shear parallel to the layers, which reduces the coefficient of friction as it is proportional to the parallel layer's shear stress. It should be noted that this will only work if the lubrication layer is parallel to the sliding motion. Further improvement could also be in the form of increased adherence of the solid lubricant to the surfaces, which increases service life (Shankara et al., 2008).

This study focused on synthesising reduced graphene oxide and functionalising it via click coupling to provide an alternative and a more efficient antiwear additive to lube oil, which in turn enhances fuel economy.

2.4 An introduction to Click Chemistry

A "click" reaction binds two molecules in the presence of a catalyst. It is also a green process, as per Kolb, Finn and Sharpless (2001). The study further showed that the reaction is one that is highly selective and capable of producing high yield at mild conditions with excellent water tolerance. The most commonly used catalyst for "click" reaction is Cu^{I}, which usually involves azide/alkyne cycloaddition (CuAAC) (Iha et al., 2009; Kolb et al., 2001). A good comparison to this reaction would be the Huisgen reaction procedures, where no catalyst was used to combine acetylene dicarboxylate and phenyl azide to produce 1, 2, 3-triazoles (Huisgen, 1963). Unlike CuAAC reactions, which is selective to form 1,4-disubstituted triazoles, Figure 2.8 also shows Huisgen reaction yield 1,4 and 1,5-disubstitution products (Rostovtsev et al., 2002; Tornøe et al., 2002). The Cu^{I} catalysts lowers the activation energy barrier by changing the mechanism of reaction, as in the case of reactions between propyne and methylazide (Himo et al., 2005).

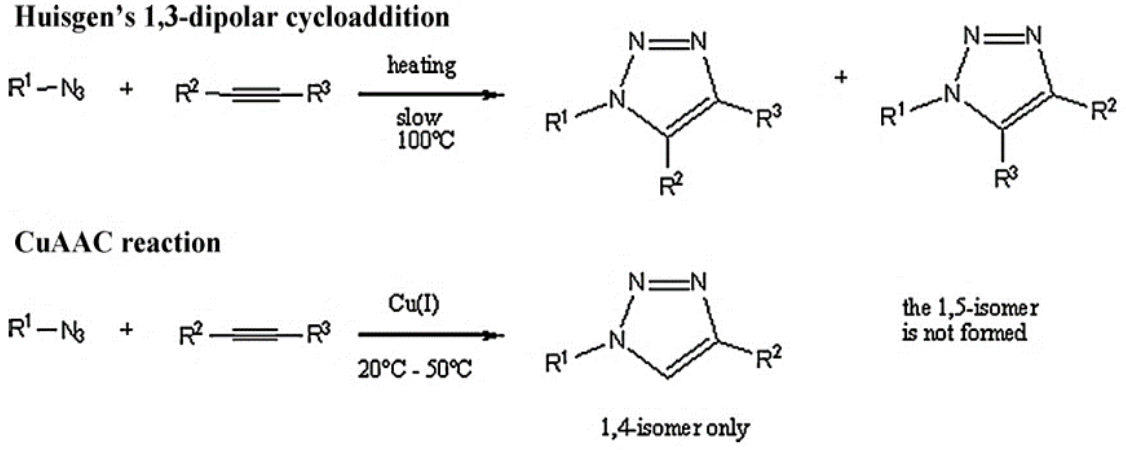

Figure 2.8: The Huisgen's and CuAAC reaction (Liang & Astruc, 2011)

Being facile and selective, CuAAC reaction was found to be reliable (Bock et al., 2006; Golas & Matyjaszewski, 2010; Hein & Fokin, 2010; Meldal & Tornøe, 2008; Rodionov et al., 2007; Sumerlin & Vogt, 2009). The wide applicability of a wide range of Cu^{I} precursors and solvents, including aqueous solvents, further promote the recognition

received by this reaction. It should be noted that there are other catalysts that can be used for the azide/alkyne cycloaddition (AAC), such as ruthenium cyclopentadienyl complexes (L. Zhang et al., 2005), Ni^{2+}, Pd^{2+}, Pt^{2+} and Au (I) (Liang & Astruc, 2011), albeit with reduced overall efficiency. The traits of click chemistry, particularly its stability from hydrolysis and dimerization, makes the reaction a viable method for upgrading carbon-based materials, such as carbon nanotubes (CNTs) (Franc & Kakkar, 2008; Lutz & Zarafshani, 2008; Mansfeld et al., 2010) and graphene oxide (Lutz & Börner, 2008; Mullen et al., 2011), which is essentially CNT's 2D counterpart.

2.4.1 Mechanism of Copper-Catalyzed Azide-Alkene Cycloaddition

The mechanism of CuAAC reaction was the highlighted in the study conducted by The Script group via kinetic studies using DFT calculations (Ahlquist & Fokin, 2007; Himo et al., 2005). The first step was lowering alkyne's pKa by 9.8 pH units during its coordination. This lead to the deprotonation of π-alkyne-Cu^{I} intermediate by water to form the σ-alkynyl-Cu^{I} species (Straub, 2007). The rate of reaction was found to be second order with respect to Cu^{+}. The cations were found to aggregate at high concentrations. There are two proposed ways by which alkynyl and azide reactants can interact with the metal centre at different or similar metal sites as illustrated in Figure 2.9 (Rodionov et al., 2007).

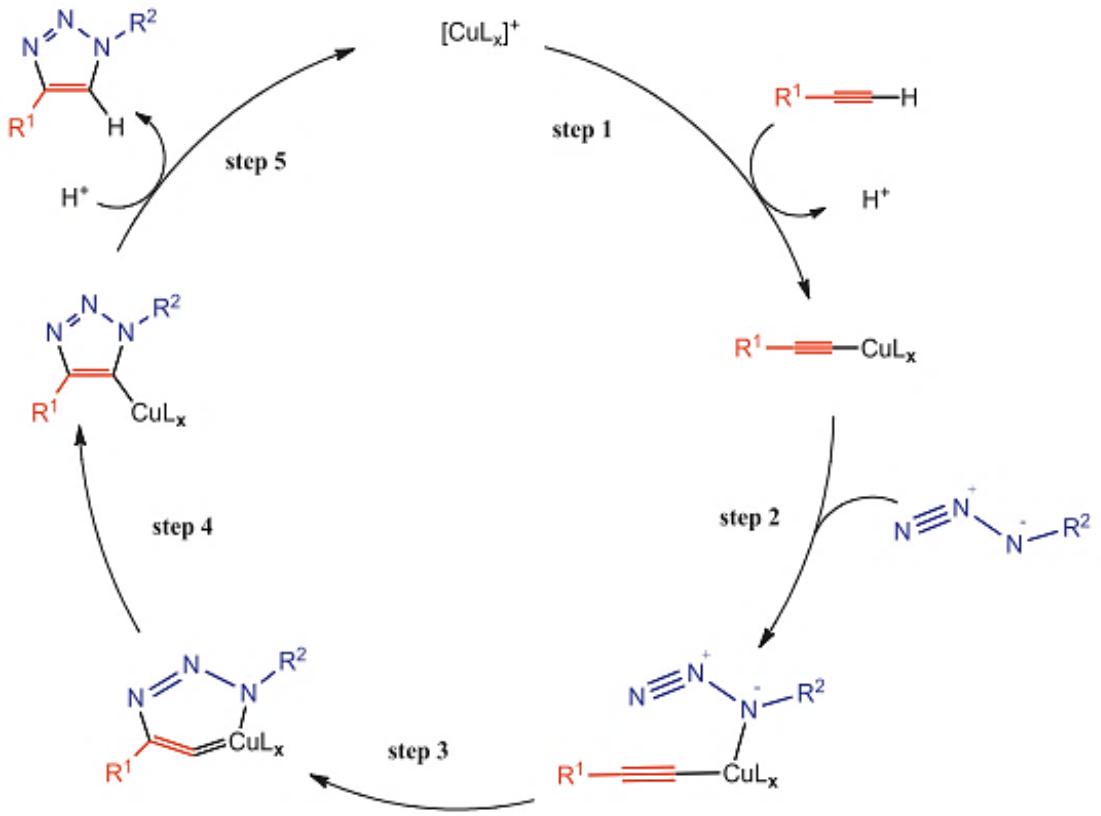

Figure 2.9: Proposed catalytic cycle for the CuAAC reaction based on DFT calculations (Hein & Fokin, 2010)

In the bimetallic route, the decreasing electron density on the sp carbon atoms lead to the enhancement of the reactivity of the alkynyl ligand. This in turn leads to the σ-alkynyl-Cu^{I} species to undergo π-complexation calculation from the DFT modelling, conformed to a reaction between a second Cu^{+} atom and Cu^{I}-acetylide (Ahlquist & Fokin, 2007; Rodionov et al., 2007). This is then followed by an attack by the azide group, and Cu^{III} vinylidene metallacycle formed as a product of this. The crux of this mechanism is the proposed formation of μ_2-ligande $\sigma-\pi$-alkynyl dicopper transition state, shown in Figure 2.10 (Hein & Fokin, 2010).

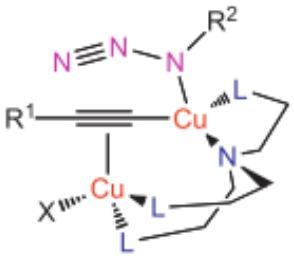

Figure 2.10: Alkyne-bridged bimetallic species (Hein & Fokin, 2010)

2.4.2 CuAAC reaction with GO

Click chemistry has been widely used to introduce functional group to a material to tailor its properties for specific tasks (Salvio et al., 2009; Sun et al., 2010). This provide new platforms for improving the 2D macromolecule via the introduction of moieties, which alters the physicochemical properties. Further probing is required to fully understand the conditions and depth of this method's applicability, especially in the context of further improving GO. Table 2.1 tabulates reviews on functionalisation of GO via click chemistry.

Table 2.1: Review on functionalization of GO via Click Chemistry

Year	Review on click reaction with GO	References
2010	Kou and co-worker reported the anchoring of poly (ethylene glycol) on nanosheets of 2D graphene oxide via click chemistry to improve solubility in organic solvents.	(Kou et al., 2010)
2011	Pan et al. demonstrated achieved the grafting a well-defined poly(N-isopropylacrylamide) via click chemistry as an effective transport for anticancer drug delivery. The functionalized graphene sheets were shown to have thermo-sensitivity post-grafting.	(Pan et al., 2011)
2012	Ye et al. analysed variety of methods to graft dispersed graphene nanosheets. The methods' efficiency and versatility were also presented.	(Ye et al., 2012)

Table 2.1, continued

Year	Review on click reaction with GO	References
2014	Nia et al. reported the synthesis of a well dispersed copper nanoparticles supported on layers of graphene nanosheets. The material was then used as a catalyst to achieve Cu(I)-catalyzed [3+2] cycloaddition with commendable reactivity.	(Nia et al., 2014)
2015	The synthesis of polypyrrole-grafted graphene sheets with good conductivity was used in a resistive-memory-based application, which involved compounds of low volatility was reported by Ramasamy and co-worker.	(Ramasamy et al., 2015)
2016	Han and Cho studies the click coupled stitched GO sheets by using a click chemistry reaction. The synthesized material was then used fillers for in polymer nanocomposites. The material also demonstrated capability as photothermal fillers.	(Han & Cho, 2016)

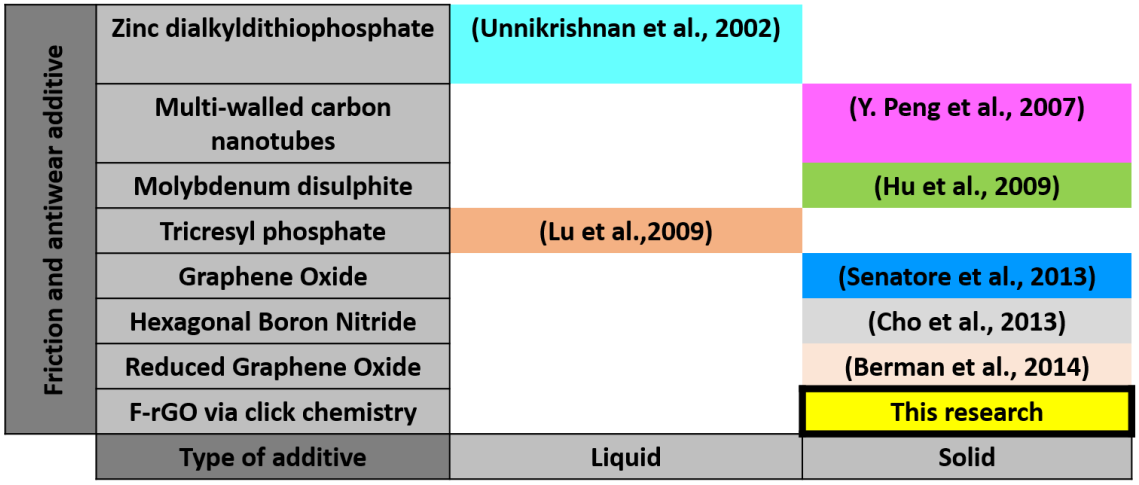

Figure 2.2.11: Research gap between literature studies and current research

CHAPTER 3: RESEARCH METHODOLOGY

This chapter will be partitioned into three sections with the first section describe the synthesis procedures of functionalized rGO. The second section covers the experimental techniques used to characterise the F-rGO additives where the third section appears to investigate the physicochemical and tribological properties of the additives in base oil as alongside it's working mechanism. The research methodology design is shown in Figure 3.1.

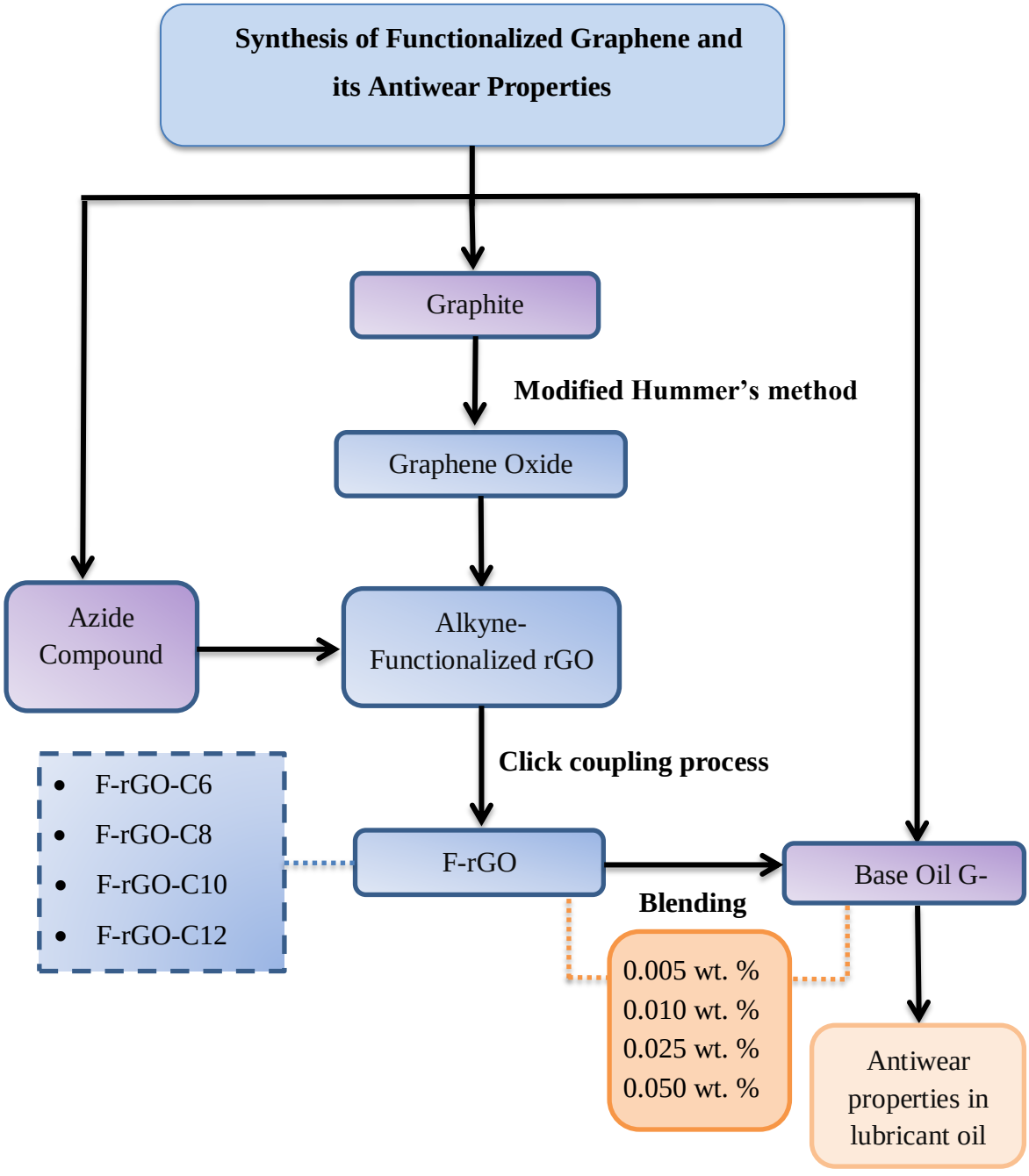

Figure 3.1: Research methodology design

3.1 Materials

All of the chemical reagents used in this work were of analytical grade and utilised without further purification. The materials used in this work are listed in Table 3.1.

Table 3.1: List of chemicals used in this study

Name	Molar mass (g/mol)	Brand
Flakes of graphite	12.00	Asbury Graphite Mills, Inc.
Sulfuric acid (H_2SO_4) (98 %)	98.08	Sigma Aldrich
Phosphoric acid (85 %) (H_3PO_4)	98.00	Sigma Aldrich
Hydrochloric acid (HCl) (37 %)	36.460	Sigma Aldrich
Hydrogen peroxide (H_2O_2) (30 %)	34.01	Merck
Potassium permanganate ($KMnO_4$)	158.03	Merck
Sodium azide (NaN_3)	65.01	Sigma Aldrich
Dimethyl sulfoxide (DMSO)	78.13	Friendemann Schmidt
Tetrahydrofuran (THF)	72.11	Sigma Aldrich
Lithium aluminum hydride ($LiAlH_4$)	37.95	Sigma Aldrich
1-bromohexane	165.07	Sigma Aldrich
1-bromooctane	193.12	Sigma Aldrich
1-bromodecane	221.18	Sigma Aldrich
1-bromododecane	249.23	Sigma Aldrich
Methyl-3,5-dihydroxybenzoate	168.15	Sigma Aldrich

3.2 Sample preparation

3.2.1 Synthesis of graphene oxide

The modified Hummer's method was used to synthesise GO via exfoliation. Exfoliation of the pre-oxidised graphite powders into sheets of GO was achieved using the following approach: 120 mL of H_2SO_4 was mixed with 13 mL of concentrated H_3PO_4. This was followed by the addition of 1.0 g graphite powder and continuous stirring. After 10 minutes, gradual addition of 6.0 g of $KMnO_4$ was gradually added to the solution, while the temperature was kept lower than 10 ^oC to prevent overheating. The mixture was stirred at 10 ^oC for an hour. The newly formed solution was diluted and cooled, while continuously stirred. The suspended material was then treated with a solution of 30 % H_2O_2 (20 mL). The mixture was centrifuged thrice with HCl to remove any remaining Mn^{2+} in the GO. Finally, the resultant GO was washed 6 times with DI water, then filtered, sonicated, and dried to obtain graphene oxide sheets.

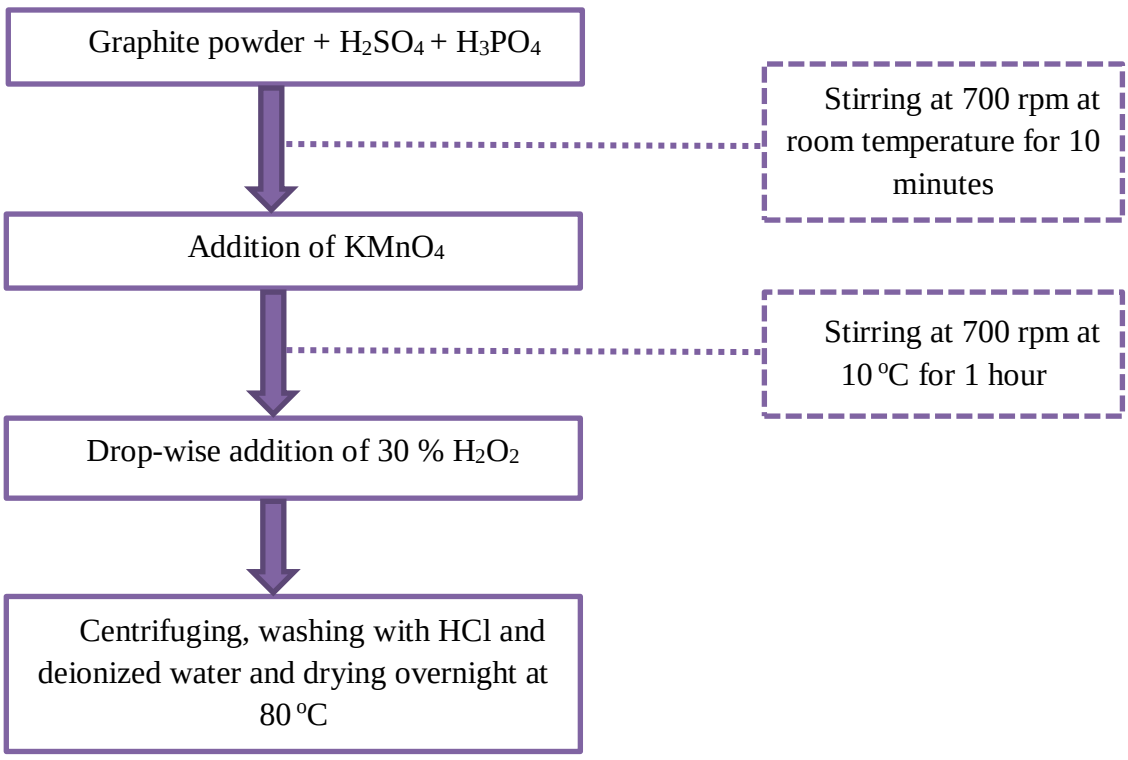

Figure 3.2: Flow chart for the synthesis of GO

3.2.2 Synthesis of Alkyne-Functionalized rGO Compound

3.0 g of Methyl-3,5-dihydroxybenzoate was dissolved in acetonitrile. This was followed by introducing 7.4 g Potassium carbonate and 4 mL of propargyl bromide (80 wt. % in toluene) to the mixture, which was thereafter refluxed at 80 ^{o}C for 24 hours, filtered, then evaporated to obtain yellow flakes. Afterwards, 0.9 g of $LiAlH_4$ was added to 3.0 g of this flake in THF. The mixture was stirred for 24 hours, then the $LiAlH_4$ was quenched dropwise via the addition of water, followed by being filtered and dried over anhydrous $MgSO_4$ to form an alkyne compound. Afterwards, 1.0 g of GO was stirred in chloroform, followed by dropwise of thionyl chloride and triethyl amine, and stirred for 2 hours, then evaporated to form chlorinated functionalized GO. 1.0 g of the alkyne compound, 1.0 g of the chlorinated functionalise GO, and 0.13 g of sodium hydride was mixed in THF at 5 ^{o}C, and stirred for 24 hours to obtain alkyne functionalized GO.

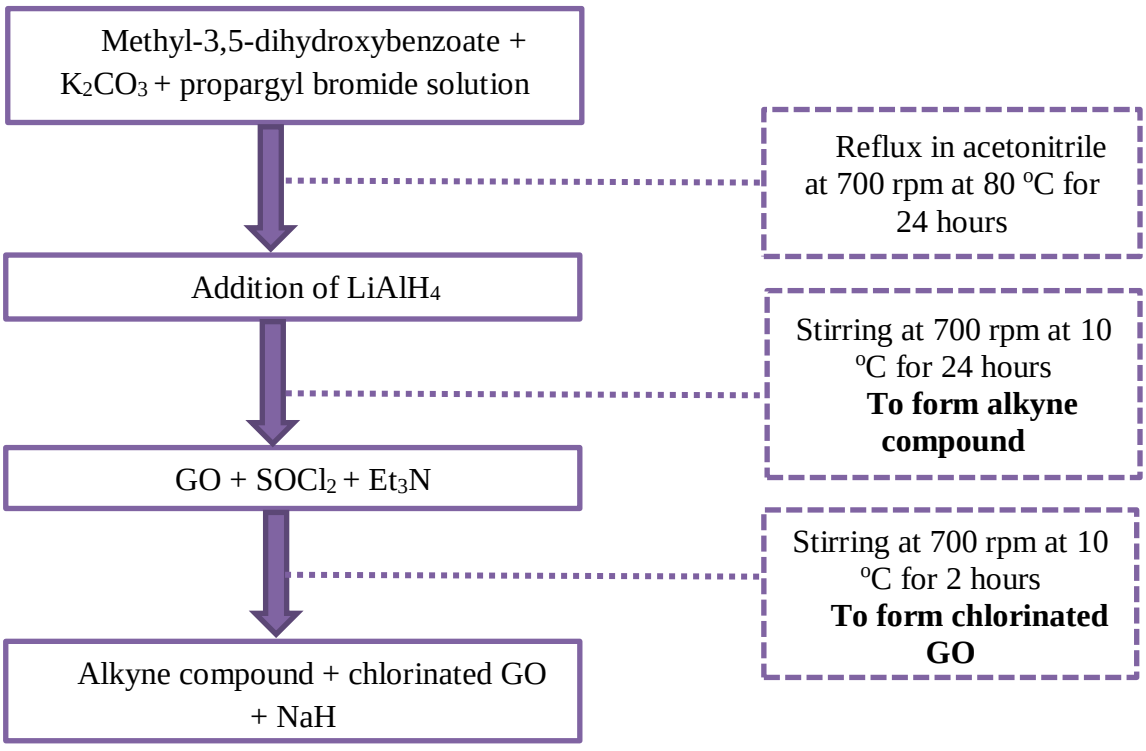

Figure 3.3: Flow chart for the synthesis of alkyne-functionalized rGO

3.2.3 Synthesis of Azide Compound

The synthesis of Azide compound involved mixing 4.0 g of sodium azide and 4.2 mL 1-bromohexane in DMF. The reaction was conducted under reflux for 24 hours at 80 ^{o}C. The product was then extracted with diethyl ether and washed with water. Excess water was removed via the introduction of anhydrous $MgSO_4$, which was then evaporated. The reaction was repeated with 1-bromooctane, 1-bromodecane, and 1-bromododecane.

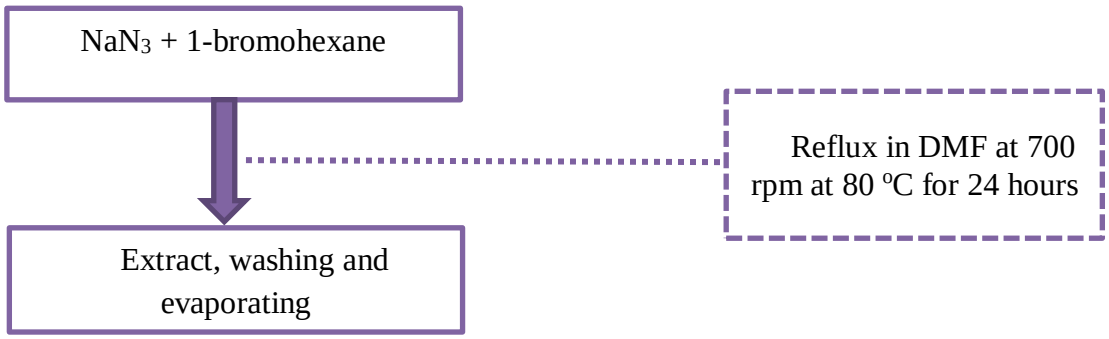

Figure 3.4: Flowchart for the synthesis of azide compound

3.2.4 Synthesis of Functionalized GO via Click Chemistry

Functionalized GO was synthesized using Click Chemistry. 0.01 g of Alkyne-functionalized GO, 0.02 g 1-azido hexane, 0.1 g of sodium ascorbate, and 0.2 g copper (II) sulphate were dissolved in a mixture of DMSO and distilled water, then stirred overnight. The mixture was then filtered and washed congruently with distilled water and ethanol, and vacuum dried for 24 hours.

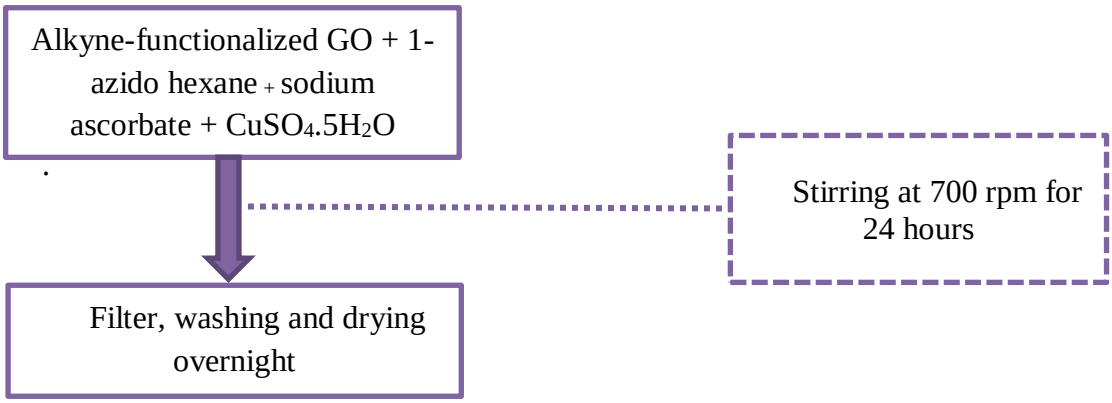

Figure 3.5: Flowchart for the synthesis of F-rGO

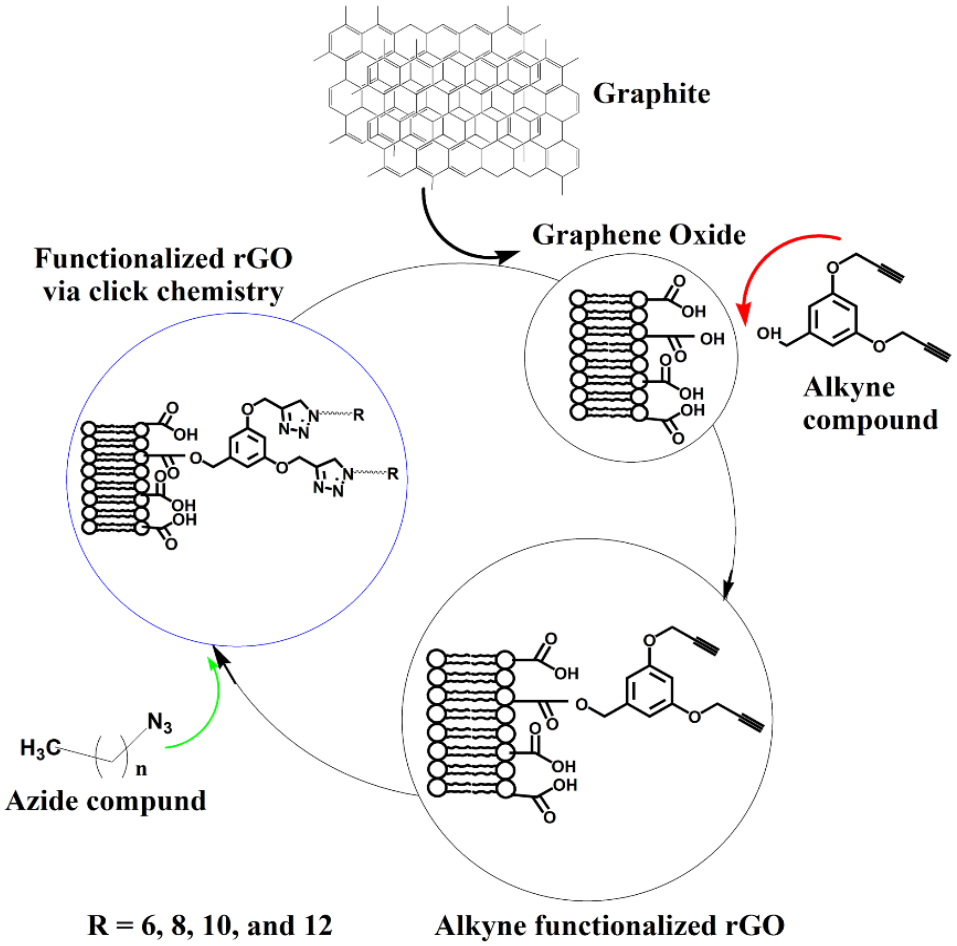

Figure 3.6: General procedure for F-rGO

3.3 Characterisation techniques

This section describes the characterisation techniques used in this work, which includes techniques such as Fourier Transform Infrared (FTIR), Raman, X-ray Photoelectron Spectroscopy (XPS), Thermogravimetric Analysis (TGA), and X-ray Diffraction (XRD) for analysing the elemental composition, TGA to study weight loss as a function of temperature, and Field Emission Scanning Electron Microscopy (FESEM) to determine the morphologies and dimensions of the nanocomposites. Each of these studies combine to give an overall characterisation of the synthesized F-rGO along with their variation of physicochemical properties with respect to one another as well as from the base material, GO. This bring about the isolation of F-rGO with most desirable features as well as highlighting their advantages in the tribology field.

3.3.1 Fourier Transform Infrared (FTIR) Spectroscopy

FTIR spectroscopy techniques utilises infrared wave bombardment to the material under analysis. The absorbance or the emission wave will then be subjected to the mathematical conversion known as Fourier Transformation to yield their respective spectrum which can then be interpreted. This method of analysis allows for identification of functional groups present in the sample under study and in this research the analysis allowed identification of functional groups present in the GO and F-rGO. This allows the distinction of the two materials from one another, as well as confirming the functionalisation of the GO based on the functional groups present.

In this study, Perkin Elmer FTIR spectroscopy was used to identify the F-rGO functional groups between 400 to 4000 cm^{-1} for each set of samples as shown in Figure 3.7. The samples were prepared using the potassium bromide (KBr) method, where 0.03 mg of F-rGO was mixed with 4 mg of KBr. The trituration of KBr helps prevent light scattering due to the large size of the KBr crystals. The mixture was then formed into a pellet, which was then held in place by a sample holder, which enables the uninterrupted passage of the IR beam.

Figure 3.7: Perkin Elmer Instrument FTIR for chemical bonding studies (Elmer, 2017)

3.3.2 Raman Spectroscopy

Raman spectroscopy applies similar concept as to FTIR analysis, except the scattered energy is measured rather than the absorbed or emitted energy. Raman shifts come about from the inelastic scattering of the incident energy wave which come in the form of Stokes or anti-Stokes scattering. When the electromagnetic radiation interacts with polarisable electron cloud in a molecule the excitation of the electron takes place which then lead to the said energy scattering. The shift in the energy caused by the energy loss due to inelastic scattering is measured as Raman shifts, which is unique from one molecule to another.

The Raman spectra were obtained using a Renishaw inVia Raman microscope shown in Figure 3.8, with a 514 nm laser as its excitation source within the range of 100 - 3000 cm^{-1}. To obtain the F-rGO spectra, 0.05 g of F-rGO was tested using a 0.02 mV laser power and 180 seconds of exposure time. The obtained Raman spectra was analysed to determine the phases of the F-rGO.

Figure 3.8: Renishaw inVia Raman Microscope for structural characterisation (Renishaw, 2017)

3.3.3 X-ray Photoelectron Spectroscopy (XPS)

The underlying concept behind this analysis is the quantisation of energy, which is unique for bonded electron in different form of matter. Similar to other spectroscopy method, the analysis begins with bombardment of the sample with electromagnetic radiation, in this case X-ray. This leads to excitation of the electron, which also leads to the emission of the electron. With the fact that the binding energy for each compound is different, particularly if the atom is bonded differently, the energy can be used to identify different atoms present on the surface of the sample.

X-ray photoelectron spectroscopy provides an in-depth information of the chemical state of elements found on the surface of F-rGO. This pointed to the specific bonding of the elements present on the surface of the said material. The analysis is carried out at an average depth of 5 nm. Figure 3.9 shows the ULVAC-PHI Quantera II, with a 32-channel spherical capacitor, analyses the energy re-emitted from the material after bombardment by X-ray under vacuum condition (1×10^{-6} Pa). The process also utilises hemispherical analyser with a natural width of 680 meV and monochromatic Al K_α sources (1,486.6 eV).

Figure 3.9: ULVAC-PHI Quantera II for surface analysis (ULVAC-PHI, 2017)

3.3.4 X-Ray Diffraction (XRD) Analysis

The crystallographic structure and phase of the F-rGO was investigated using X-ray diffraction (XRD) analysis. In this research, the XRD diffractograms of the solid powder was analysed using Bruker D8 Advance diffractometer as per Figure 3.10, equipped with a quartz monochromatized Cu K_α radiation and wavelength, $\lambda = 0.154059\, nm$. Approximate 1 g of the sample was measured and placed into the sample holder. The system operated at a scanning rate of 0.02º per second to over a 2θ range of 10º to 80º. Other frequent applications of XRD is to determine the crystallite size. The Debye-Scherrer equation can be used to obtain an estimated nanoparticle size. There are several studies on the determination of the crystallite size from XRD patterns using the Debye Scherrer's equation:

$$\boldsymbol{D = \frac{K\lambda}{\beta cos\theta}} \qquad \textbf{(Equation 3.1)}$$

where;

K = shape factor,

λ = wavelength of x-ray,

β = band broadening at half of the maximum intensity of each peak,

θ = Bragg angle,

D = average diameter of the domains.

Figure 3.10: Bruker D8 Advance diffractometer for crystal structure and composition studies (Bruker, 2016)

3.3.5 Thermogravimetric Analysis (TGA)

TGA elucidates the composition of F-rGO and thermal stability as a function of temperature and time. It records the change in the weight of the F-rGO with increasing temperature and time under the flow of Argon gas. For compositional analysis, TGA helps estimate the amount of each component in the material by calculating the onset temperature of degradation or volatilisation. In this work, TGA measurement was performed using a Mettler Toledo, TGA/SDTA-851^e shown in Figure 3.11 that operates over the temperature range of 20 - 1000 °C and a scan rate of 20 °C/min. The sample was in the powder form, as it has a larger surface area, which helps improve the weight loss resolution and temperature reproducibility.

Figure 3.11: Mettler Toledo, TGA/SDTA-851^e thermal analyser to study the rate of change in weight over temperature or time (Toledo, 2016)

3.3.6 Field Emission Scanning Electron Microscopy (FESEM)

The surface features and particles sizes or shapes of the sample were analysed using a high-resolution field emission scanning electron microscope. The process begins with the irradiation of the samples with electrons and the reflected energy is used to image the surface at microscopic level. In this research, the morphology of the F-rGO was determined using a scanning electron microscope Quanta FEG 450 shown in Figure 3.12. The field emission gun electron source of this model produces a high current, which enables imaging up to 3 nm resolution and a magnification of up to 250,000 ×. All the tested samples were in the powder form.

Figure 3.12: Quanta FEG 450 FESEM for morphology and structural study (Scientific, 2016)

3.4 Physicochemical measurement of additives

F-rGO samples were introduced into the base oil via mechanical stirring, coupled with sonication shown in Figure 3.12. Base fluid used in this research is base oil group 3 (G-III) since it is the best grade and purer of petroleum base oil. Synthesize functionalized rGO via click chemistry with different alkyl terminal chain with the concentration of additives is 0.010 wt. % and formulate base oil lubricant using various additives concentration are shown in Table 3.2 and Table 3.3.

Table 3.2: Additives with different alkyl-chain

Sample	Additives (wt. %)	Base oil G-III (wt. %)
Base Oil G-III	0.00	100
F-rGO-C6	0.010	99.99
F-rGO-C8	0.010	99.99
F-rGO-C10	0.010	99.99
F-rGO-C12	0.010	99.99

Table 3.3: Formulation of lubricant oil with additive in varying concentration

Additives (wt.%)	Base Oil G-III (wt. %)
0.005	99.995
0.010	99.990
0.025	99.975
0.050	99.950

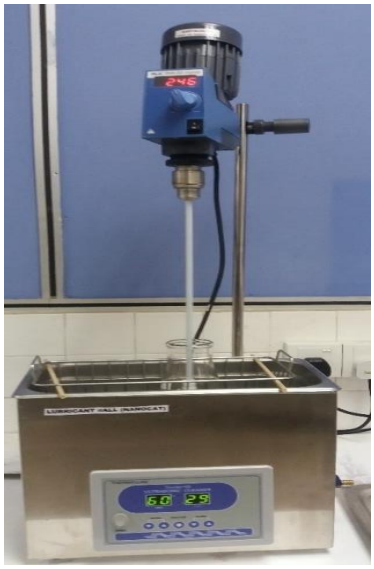

Figure 3.13: Oil blending process

3.4.1 Density Analysis

The density and/or relative density of distillates of the petroleum and oils of varying viscosity were determined at test temperatures of 15 – 35 °C. The restriction imposed on such application lies within vapour pressure of less than 600 mm Hg (80 kPa) and a measured viscosity of less than 15,000 cSt (mm^2/s) in terms of temperature during testing.

3.4.2 Viscosity Analysis

Viscometer is used to measure the viscosity of a fluid which measure under one flow condition. The Anton Paar viscometer is a built-in density measurement based on the oscillating U-tube principle that allows the determination of kinematic viscosity from the measured dynamic viscosity employing the relation:

$$\boldsymbol{v = \frac{\eta}{\rho}} \qquad \textbf{(Equation 3.2)}$$

where;

$\boldsymbol{v}$ = the kinematic viscosity (mm^2/s)

η = the dynamic viscosity (mPa.s)

ρ = the density (g/cm^3)

The viscosity analysis of functionalized rGO were carried out using SVM™ 3000 Stabinger Viscometer shown in Figure 3.14 from Anto Paar which determines dynamic viscosity, kinematic viscosity and density of oil as well. The viscosity measurements were conducted at 40 °C and 100 °C, while the viscosity index (VI) was determined based on ASTM D445 and ASTM D2270. VI is used to measure the temperature dependence of an oil's kinematic viscosity, and the higher the VI, the lesser the change of viscosity of the oil with temperature, and vice versa.

Figure 3.14: SVM™ 3000 Stabinger Viscometer (Paar, 2017)

3.4.3 Total acid number (TAN) Analysis

The standard method ASTM D664 (Javidialesaadi & Raeissi, 2013) was used in this analysis. 0.1 M of potassium hydroxide (KOH) was used to neutralise acid component in the samples for potentiometric titration as shown in Figure 3.15. Subsequent titrations involving a mixture of toluene, isopropanol, and water (500:495:5) was carried out. The obtained value of acidic constituents was collected and reported in terms of mg of KOH for every gram of oil. Each analysis was repeated thrice to obtain an average.

Figure 3.15: Metrohm potentiometric titration (Metrohm, 2017)

3.5 Tribological analysis

3.5.1 Friction and wear test

The four-ball wear tester as shown in Figure 3.17 were utilised for testing the effect of additives to the performance of the subsequent lubricants. A 27 mm diameter stainless-steel ball bearings were exposed to the following conditions as illustrated in Figure 3.16: 1200 rpm speed under a constant load of 40 kg (392.266 N) at an elevated temperature of 35 ^{o}C. Readings were recorded every 30 seconds, and then averaged.

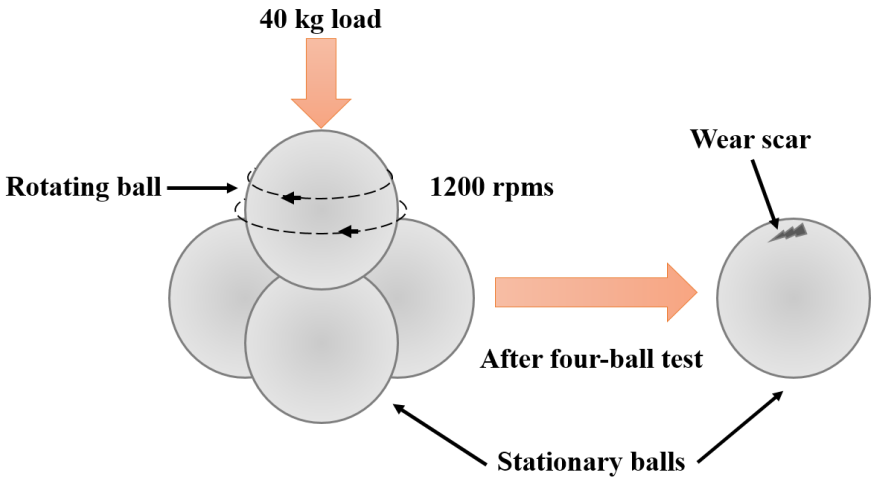

Figure 3.16: Coefficient of friction and ball wear mechanism

The four-ball test was performed thrice, and the average values of the tests are reported. The sliding wear losses were measured using a highly precise digital weighing machine. The weight losses of the test samples were then converted to volume losses. The specific wear rates were calculated using the Archard equation:

$$\boldsymbol{W\,s\ =\ \Delta V\,L \bullet d} \qquad \textbf{Equation 3.3}$$

where;

Ws = specific wear rate (m^2/N),

ΔV = loss of volume (m^3),

L = normal load (N) and

d = distance during sliding motion (m).

Figure 3.17: Four-ball tester (Instruments, 2017)

CHAPTER 4: RESULTS AND DISCUSSIONS

This chapter will discuss the results of the research. The results for both additives characterization and performance will be presented, analyzed, and compared with those reported in literature.

4.1 Sample characterization

4.1.1 Vibrational harmonic modes of F-rGO additive

The vibrational mode of the synthesized additives was studied using the FTIR and Raman spectroscopy method. The results detail the intrinsic properties of the materials. Figure 4.1 shows the FTIR spectra of edge plane functionalized reduced Graphene oxide, and show representative peaks centred at 3237, 1710, 1614, 1230 and 1044 cm^{-1}, corresponding to O–H stretching, C=O stretching, C=C stretching, epoxy C–O stretching, and alkoxy C–O stretching functionalities of graphene oxide, respectively (Choi et al., 2010; Jang et al., 2014). After the click coupling reaction, the vibration peak centred at 1710 cm^{-1}, for C=O stretching disappeared; suggesting the incorporation of the alkyl group at the edge plane (Sun et al., 2010). However, as shown in the region coloured red, the intensity of the vibration peak at 3237 cm^{-1} decreased significantly, whereas two prominent new peaks at ~2850 and ~2950 cm^{-1} appeared; this suggest C–H stretch in the $–CH_2$ of the alkyl. After click coupling, the attachment of azide groups to the surfaces of F-rGO is confirmed from the appearance absorption peak of azide groups at 2098 cm^{-1} at the region coloured yellow. The disappearing peak at 2098 cm^{-1} and the presence of the at 1100 cm^{-1} is related to the stretching of C-O groups, which proves the successful azide-alkyne coupling (Kou et al., 2010), as shown in the region coloured green.

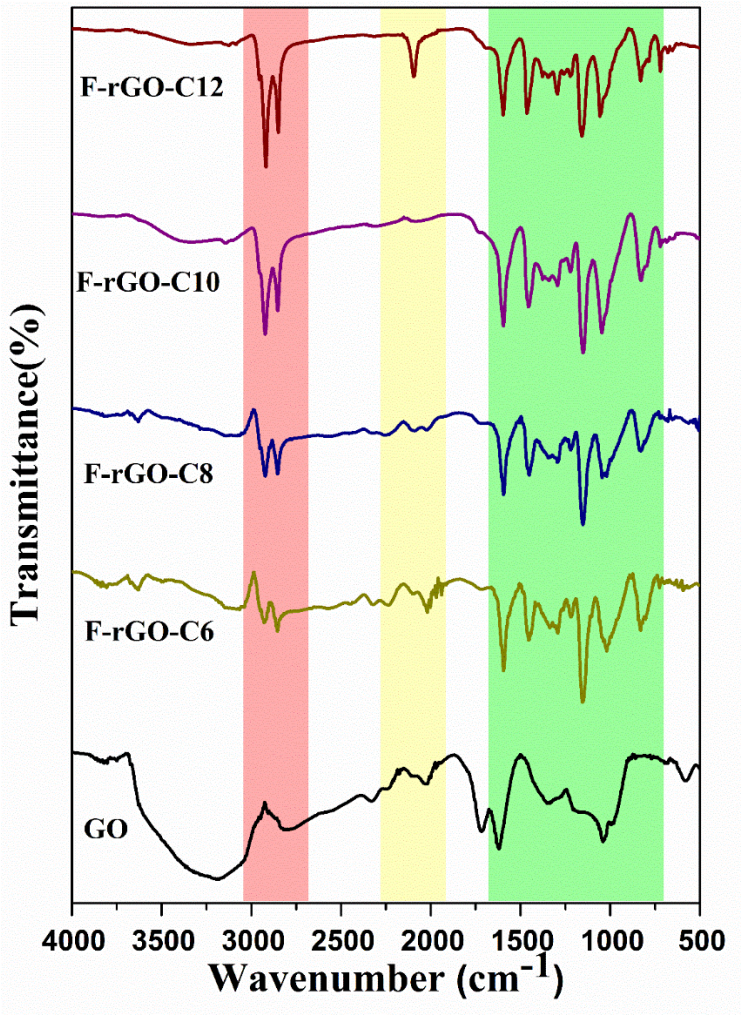

Figure 4.1: FTIR spectra of the synthesized additives

Table 4.1: FTIR band assignment for the synthesized additives

Graphene Oxide		Functionalized rGO	
FTIR band position (cm^{-1})	**Assignment**	**FTIR band position (cm^{-1})**	**Assignment**
3237	-OH	2850	C-H
2796	C-H	2098	N=N=N
1710	C=O	1590	-CONH
1614	C=C	1615	C=C
1230	C-O epoxy ring	1291	C-O epoxy ring
1044	Alkoxy C-O	1100	Alkoxy C-O

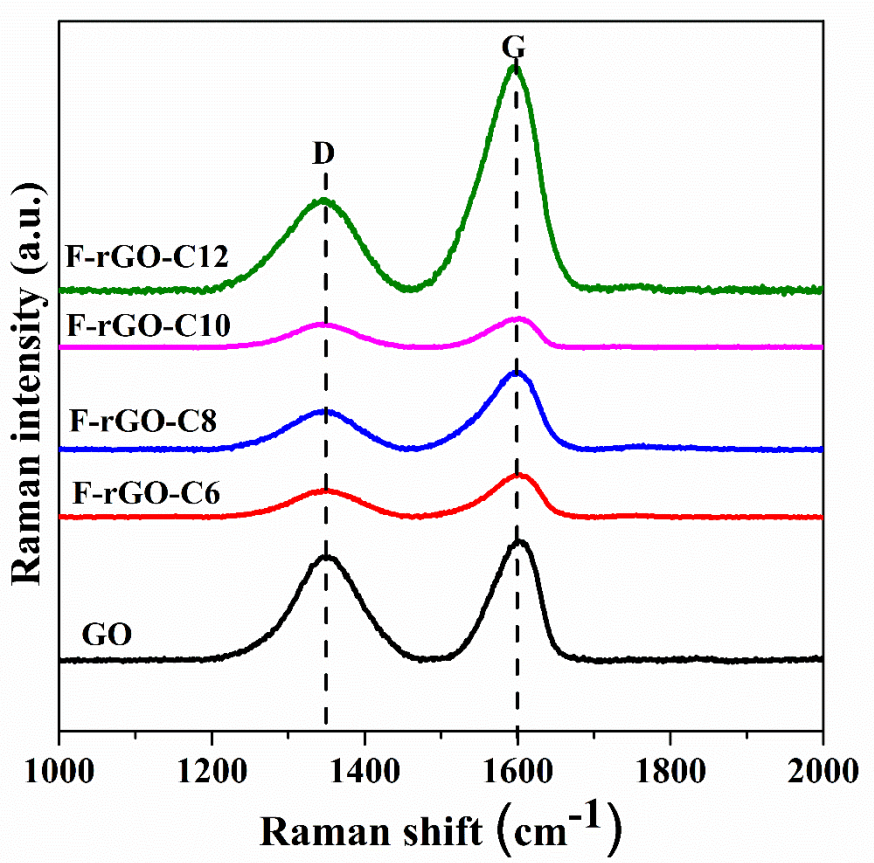

Figure 4.2: Raman spectra of GO and functionalized rGO

In Figure 4.2, each of the functionalized rGO samples were subjected to Raman spectroscopy analysis. The results showed two peaks at ~1340 cm^{-1} and 1600 cm^{-1}, each of which were assigned to the D band; indicating the presence of defect; suggesting the successful incorporation of the N-group and G band; E_{2g} band with sp^2 bonding attributes, respectively (Jang et al., 2014; Kou et al., 2010). It is interesting to note the general decrease in the intensity of these two peaks with increasing carbon chain length, up to 12. This indicates that as the chain length grows, the degree of disorder and stretching of the bonds decreases. This conforms to the observation from the XRD, where the alkyl group acts as a bridge that increases the rigidity between the layers of sheets of the materials. Furthermore, these trends resulted in amorphous carbon materials, which was also confirmed by the XRD. However, the trend does not apply to F-rGO-C12, which has a significantly longer carbon chain compared to the others. The intercalation between the layers of the material is covered, which increases structural disorder and bond stretching.

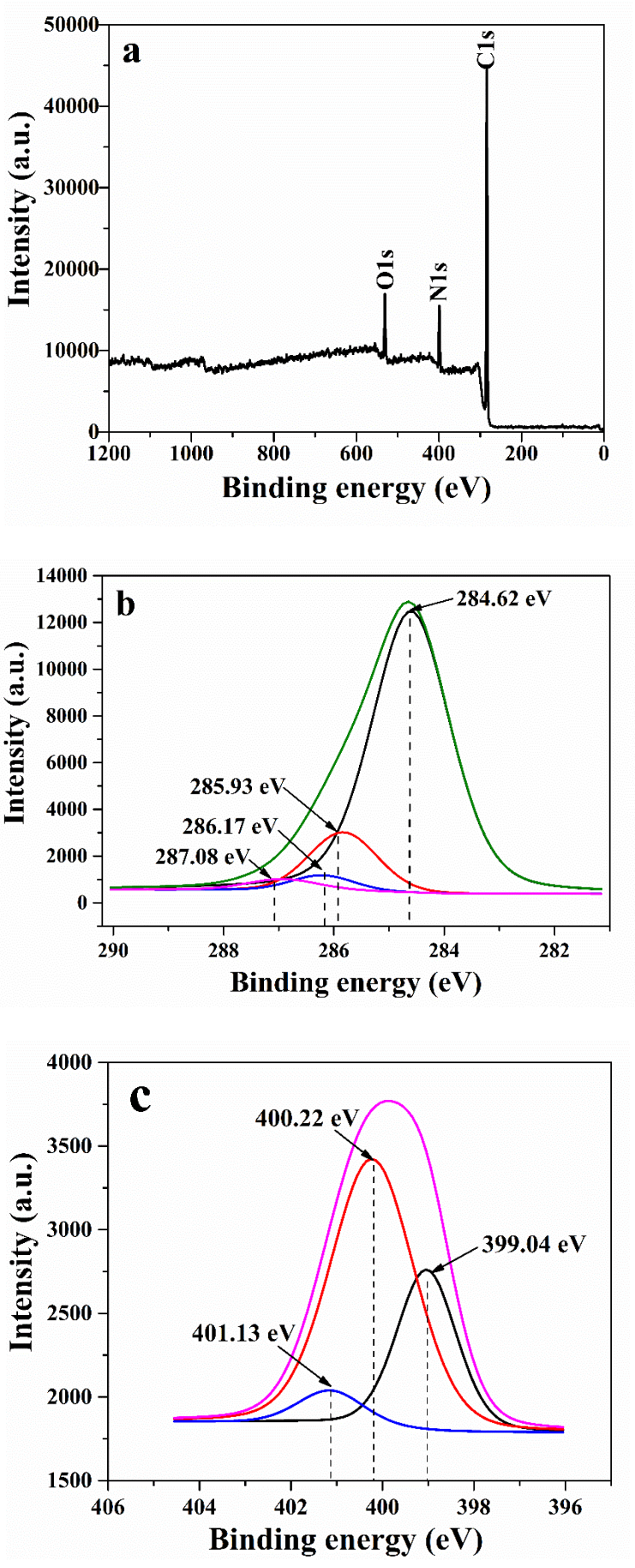

Figure 4.3: XPS spectra of (a) GO and F-rGO in wide region; (b) C_{1s} region of F-rGO; (c) N_{1s} region of F-rGO

Figure 4.3 shows further evidence of the chemical composition of the F-rGO by X-ray photoelectron spectroscopy (XPS), where the peaks correspond to C_{1s} (284 eV), N_{1s} (400 eV), and O_{1s} (531 eV), which agrees with the results reported by the FTIR. The N_{1s} peak clearly shows the nitrogen atoms as part of the formed triazole ring. The C_{1s} spectra of F-rGO in Figure 4.3(b) shows four different characteristics of carbon bonds. A broad peak at 284.7 eV corresponds to sp^2 and sp^3 C-C carbon of non-oxygenated ring. Moreover, the C-O of hydroxyl (285.9 eV), C=O of carboxyl group (286.2 eV), and O-C=O (287.1 eV) were also proven (Deetuam et al., 2014). Hence, these XPS data confirms the attachment of alkyne compound on GO sheets.

Additionally, as shown in Figure 4.3(c), the N_{1s} spectra shows a broad peak centred at 400.2 eV, which confirms the formation of triazole moiety. A well-resolved peak at ~405 eV, corresponding to the free azide group, unambiguously indicates that the azide compound was covalently attached to the rGO surface via a triazole ring (H.-X. Wang et al., 2011). We anticipated that click coupling between alkyne functionalized rGO and the azide compound may not results in a 100 % conversion, since the residue of the azide group can be detected by the FTIR measurement.

Table 4.2: Atomic concentration of F-rGO

Atomic concentration (%)		
C_{1s}	**N_{1s}**	**O_{1s}**
83.38	10.56	6.06

4.1.2 XRD analysis of F-rGO antiwear additive

Figure 4.4 and Table 4.3 showed the spectrum of GO observed two peaks at 9.158º and 26.098º, which corresponds to the planes (001) and (022), respectively (Javed & Hussain, 2015). The first of this set of peaks shows d-spacing of 9.4367 Å, while the second shows a value of 3.4100 Å. The presence of these peaks, particularly the first one is highly suggestive of the formation of GO as they are often regarded as characteristic peaks of the material (D.-D. Zhang et al., 2009). With regards to all of the functionalized sample, in general they all are amorphous in nature. This is to be expected when considering that the presence of functional alkyl groups contribute in the disruption of the structure of the base material (Marcano et al., 2010).

At a closer look, there is a significant shift in the first peak (~10º) in the F-rGO compared to GO sample. This can be attributed to the amorphisation of the F-rGO, indicated by the widening of the peak in functionalized samples. From these observations, it is therefore highly indicative that functionalization of the alkyl groups between the layers of the GO sheet had already taken place. Also noted is the decreased intensity of the functionalized samples which points to the increased exfoliation of GO into singular or multiple sheets (Cai & Song, 2007).

With regards to their crystallite size, the base material, GO has an average crystallite size of 5.4 nm, while the functionalized materials are considered amorphous. This is highly indicative of reduced crystallite size in the functionalized samples, which in turn provide further proof of the increased disorderliness of the functionalized rGO's structure (Zhou et al., 2009). These evidences strengthen the postulation that the functionalization of rGO was successful.

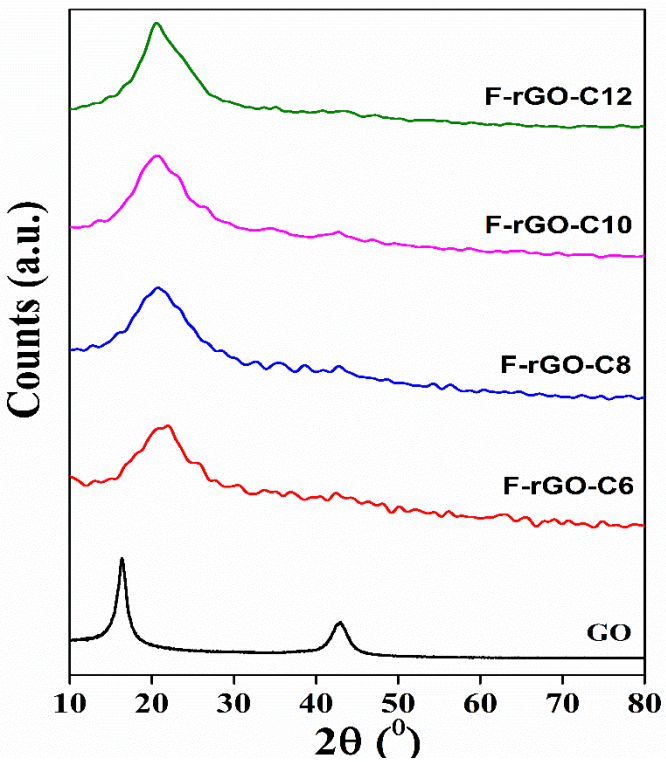

Figure 4.4: XRD spectra of the synthesized GO and F-rGO samples

Table 4.3: Summary of extract from XRD analysis

Sample	2θ	Phases	d-spacing	Crystallite size (nm)
GO	9.158°	0 0 1	9.43767	8.4
	26.098°	0 2 2	3.4100	2.4
			Average	5.4

4.1.3 Thermal stability analysis of F-rGO

Figure 4.5 shows the thermal stability of functionalized rGO forms based on their TGA plots. rGO's functionalisation does not show significant loss between 50 - 150 ^{o}C due to their hydrophobicity. Only an average of 3 % weight was lost during this period. There is also a significant drop in the weight loss between 150 - 300 ^{o}C due to the previously mentioned factor, which is attributed to oxygen based functional groups, such as carbonyl, epoxy, and hydroxyl groups (Choi et al., 2010). These groups are commonly

found on the surface of the GO, which makes up for most of the material's weight functional groups being bonded to the alkyl functional groups. This moiety decomposes between 300 - 460 ^{o}C. Grafting the alkyl functionalisation group was successfully carried out for each of the functionalized rGO materials, due to the significantly smaller amount of decomposition in the temperature range where free surface functional group were known to decompose (Kou et al., 2010). The stability of F-rGO comes from the nitrogen group decomposing at ≤ 370 ^{o}C, based on Figure 4.5. This functionalized rGO is capable of withstanding high temperatures before it loses the highly electron rich N-group, which makes it suitable for applications under 370 °C.

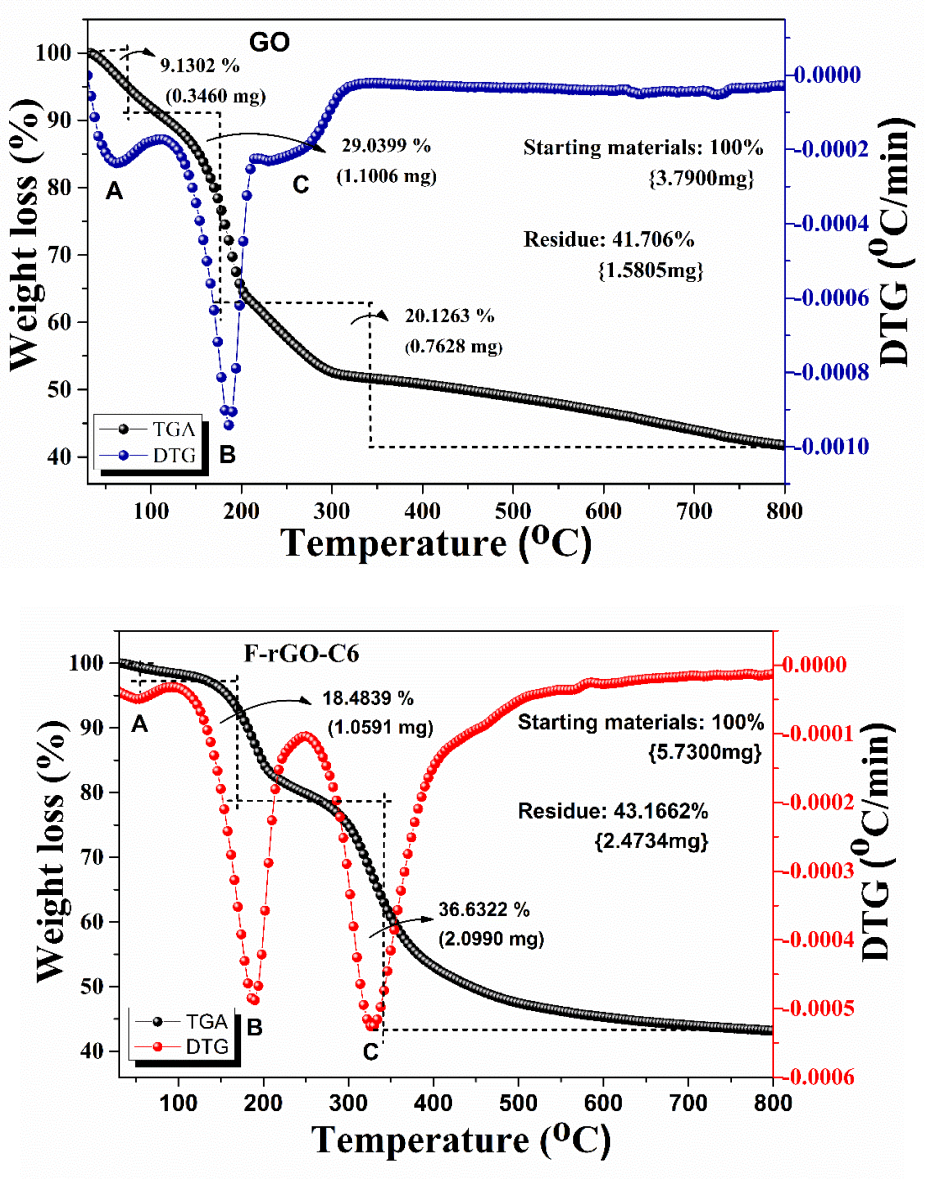

Figure 4.5: TGA and DTG traces of GO and its derivatives

Figure 4.5, continued

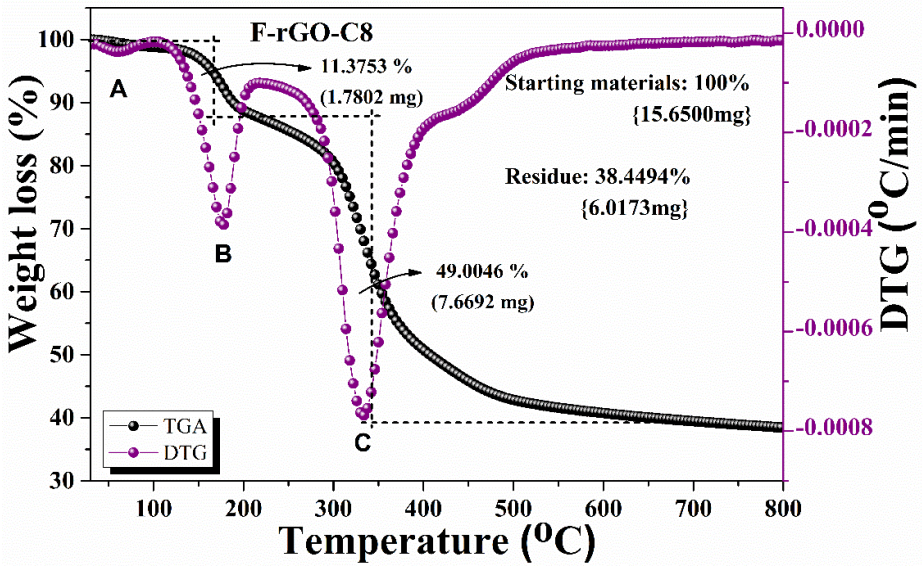

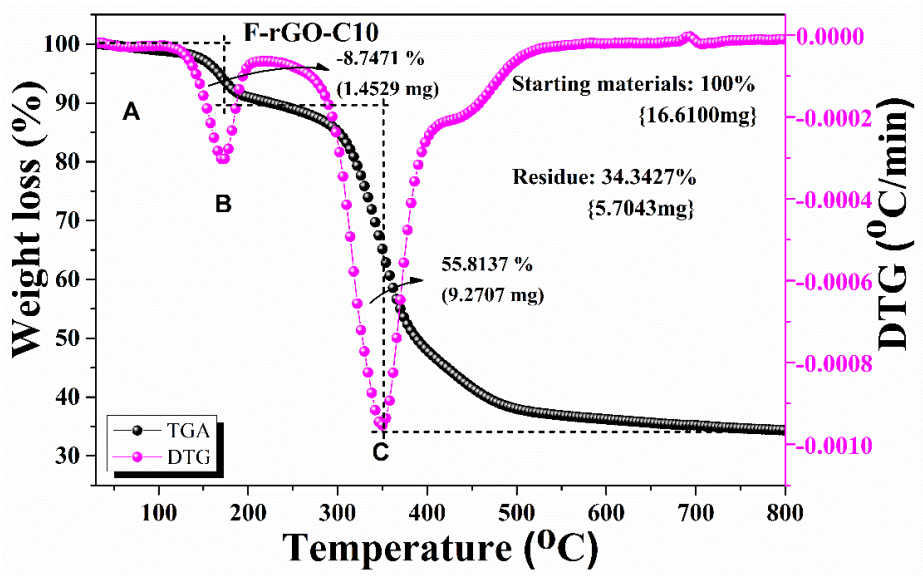

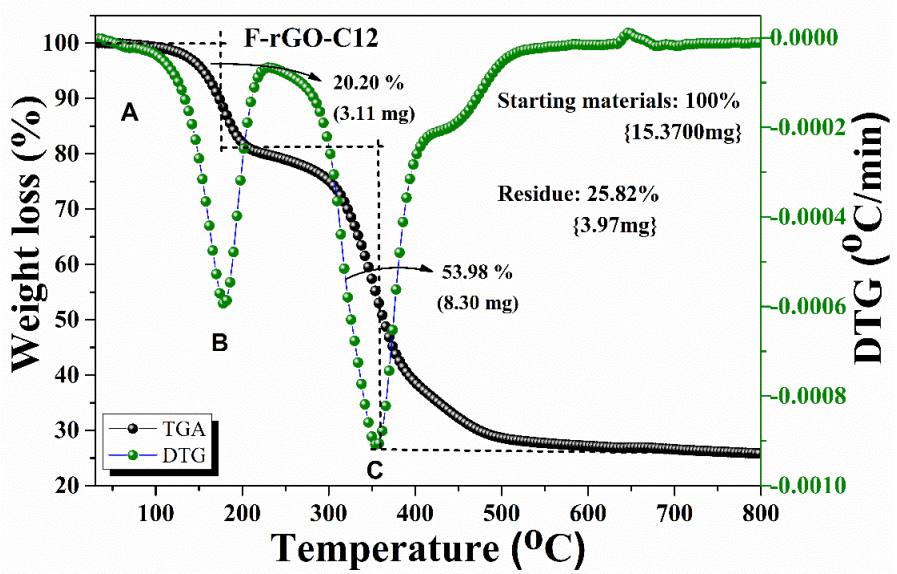

4.1.4 Morphology of F-rGO antiwear additive

Figure 4.6 showed the FESEM of functionalized rGO-C6, rGO-C8, rGO-C10, and rGO-C12. The fluffy rGO nanosheets agglomerates exhibit a dense structure of curled graphene stacking sheets (Senatore et al., 2013). The presence of these wrinkles and folds are more than likely due to the presence of the alkyl functional groups, which distorts the dense sheet found in the original structure of the GO.

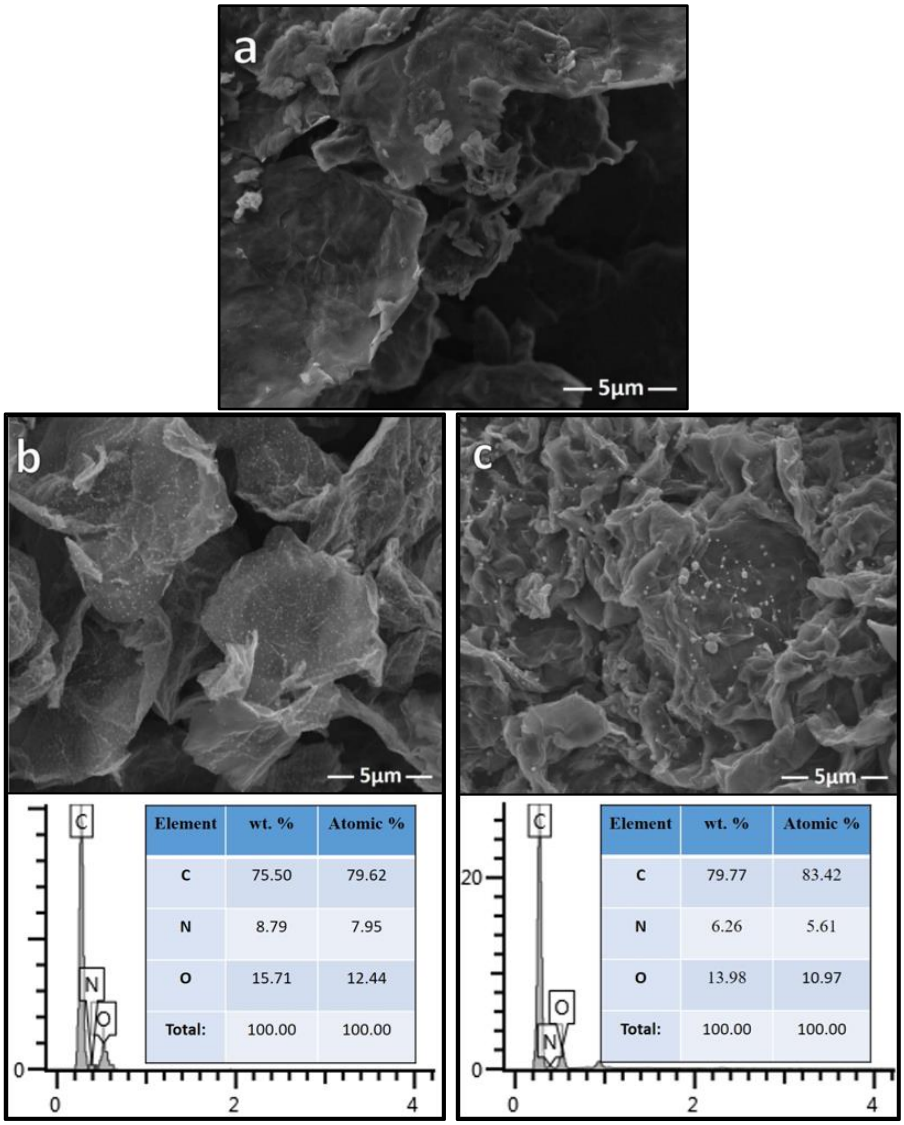

Figure 4.6: FESEM images of (a) GO; (b) F-rGO-C6; (c) F-rGO-C8; (d) F-rGO-C10; (e) F-rGO-C12

Figure 4.6, continued

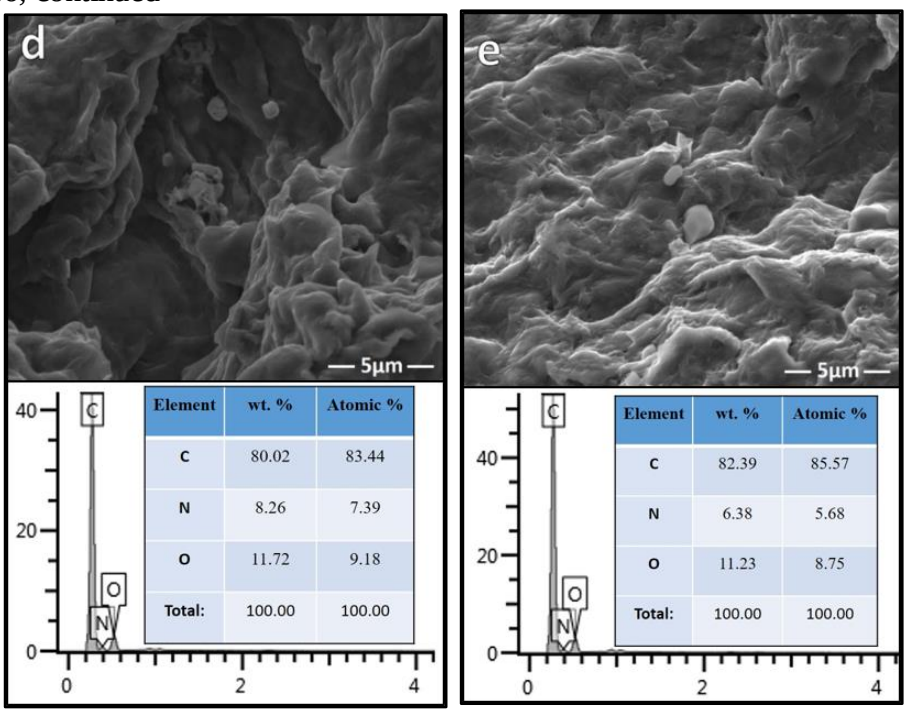

The presence of the more pronounced layers in the functionalized materials also corroborate the XRD results which point to the formation of sheets of functionalized graphene due to exfoliation resulting from the presence of the functional groups. Further evidenced here is the amorphous nature of the functionalized materials further corroborating the postulation from XRD results. This further proves that these chain act as a “spacer” that not only holds two sheets, but distorts it in a way that it folds into itself. This demonstrates that the modified Hummer’s method is able to create two-dimensional nanosheets from the exfoliated graphite precursor. The absence of Cu as indicated in the EDX spectra points to the successful elimination of the catalyst used during this modified Hummer’s method which provides further evidence to the practicality of the method.

4.1.5 Mechanism of lubrication by Functionalized-rGO-C_n

There are many evidence pertaining to the formation of graphene tribofilm when in contact with surfaces forming the basis for tear and wear reduction. These justifications only accounted for concentrations of graphene instead of the functionalized group, and it was argued that graphene is easily agglomerated due to the weak shear strength of the interlayer sliding plane disorders. These physical evidence guides the graphene- surface contact throughout its deposition on steel via the micotribometric test. On the contrary and accounting for the nanometric contacts where the contact stress is higher, it was argued that graphene could not be deposited. Recent studies attempted to solve this challenge using 100Cr6 steel ball against 316LN steel based on plastic deformation assumptions. Plastic deformation releases energy that aid physiosorbtion/chemisorption of graphene-dispersed molecules. These have been justified with the aid of hydrogen bonding linkages and participation of π bonds in graphene (Berman et al., 2015; Charlier et al., 1994; Mungse et al., 2015; A. Rasheed et al., 2016; A. K. Rasheed et al., 2015; L.-F. Wang et al., 2012; Xia et al., 2016) and the participation of electron-rich nitrogen group and alkyl chain length. This agrees with the combined effect of the π-electron. Therefore, increased length of the alkyl chain creates more contact distance between the surface, while the electron species (Nitrogen group) remain similar in all species.

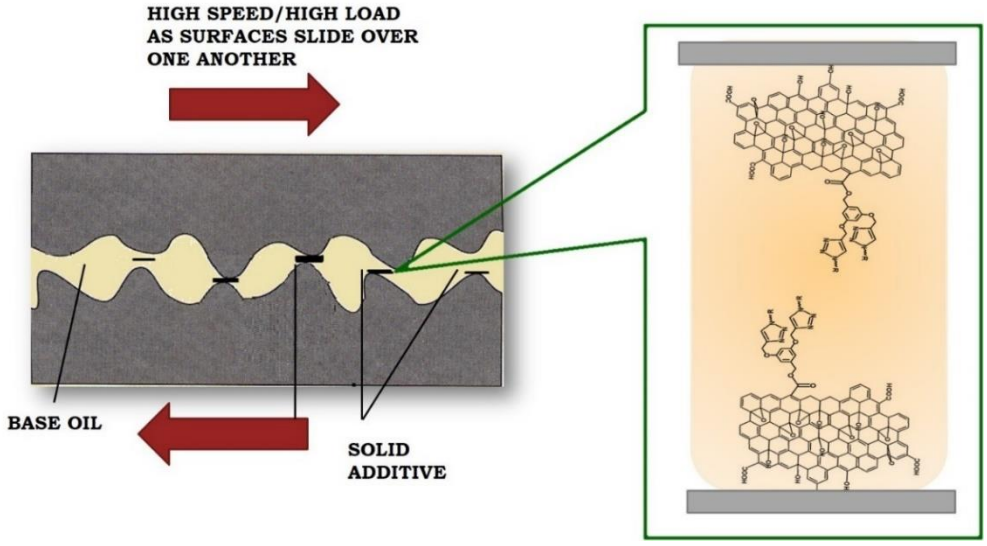

Figure 4.7: Mechanism of antiwear additive in base oil

4.2 Performance of different additive in lube oil

4.2.1 Physicochemical properties

4.2.1.1 Density Analysis

On average, the density for the base oils containing the additives with different length of carbon chains is 0.843 g/cm^3. According to Sharma et. al (Sharma et al., 2004), the density of base oil group III should be 0.825-0.847 g/cm^3 at 25 ºC. Thus, the density of base oils with additives is within the expected values for the pure base oil group III (G-III). The similar values of each set of data herein proves that the length of chain in the functionalized rGO does not affect the overall density of the lubricant oil. This is likely due to the small difference in mass contributed by the alkyl chain to their respective F-rGO. Thus, the changes are not significant enough to alter the density when the additives were added to the oil. However, the fact that the concentration for all sample were kept 0.010 wt. % of additive added should be taken into consideration. The effect when varying such concentration is illustrated in Section 4.3.1.1.

Table 4.4: Density of base oil and its F-rGO derivatives

Oil Sample	Density (g/cm^3)
Base oil G-III	0.843
G-III + F-rGO-C6	0.843
G-III + F-rGO-C8	0.843
G-III + F-rGO-C10	0.843
G-III + F-rGO-C12	0.843

4.2.1.2 Viscosity Analysis

There was a slight increase in viscosity index (VI) with increasing alkyl chain of additives, as per Table 4.5. Although the variant here is small, it can be observed clearly that F-rGO-C10 and F-rGO-C12 have the highest VI value making them the most insusceptible to changes when subjected to change in temperature. This is important as it allowed us to postulate that these two additives will be the most efficient to act as lubricant additive which are bound to be subjected to high temperature. This postulation turned out to be true as will be illustrated in the results of four-ball tests. Interestingly, these two additives contain alkyl chains relatively longer than the rest. Thus, it can be said here that the longer the chain of the hydrocarbon functional group the higher is the viscosity index, at least up until 12 carbon length. The increase in alkyl chain length increases the molecular weight which have been shown to increase stability of the overall compound to changes due to temperature (Ghosh et al., 2011).

Table 4.5: Viscosity and viscosity index of base oil and F-rGO additives

Samples	Kinematic viscosity mm^2/s		Viscosity Index
	40 ºC	100 ºC	
Base oil G-III	33.5	6.1	131
G-III + F-rGO-C6	35.7	6.4	132
G-III + F-rGO-C8	35.7	6.4	132
G-III + F-rGO-C10	35.5	6.4	133
G-III + F-rGO-C12	35.5	6.4	133

4.2.1.3 Total acid number Analysis

The data pertaining to the TAN shown in Table 4.6 show that the pure base oil and functionalized additives reported similar acid value and good results as the TAN is less than 0.10. The data also illustrates the difference in acid value pre- and post- four ball test in which all sample showed increase in the value. However, it must be noted that F-rGO-C10 and F-rGO-C12 showed smaller increase in acid number compared to the others. This is largely due to the increasing carbon chain portion of the additive, which also happens to be less susceptible to oxidation compared to the carboxyl groups present in the additive. Hence, the overall susceptibility of these two additives are lowered compared to the others due to their larger portion of oxidatively stable alkyl chain present. This confirms that there was less acidic contaminations and oxidation of the additives.

Table 4.6: Value of total acid number of base oil and F-rGO additives

Samples	TAN (mg KOH/g)	
	Before four-ball test	**After four-ball test**
Base oil G-III	0.07	0.11
G-III + F-rGO-C6	0.07	0.11
G-III + F-rGO-C8	0.07	0.10
G-III + F-rGO-C10	0.06	0.08
G-III + F-rGO-C12	0.06	0.08

4.2.2 Tribological study

4.2.2.1 Friction coefficient

A series of four-ball tests using base oil group III were carried out to study the influence of base oil on the friction performance of F-rGO additives. In this case, Figure 4.8 shows the performance results of the functionalized rGO (C6, C8, C10 and C12) material via the four-ball test analysis. F-rGO-C10 has shown superior and significant reduction of friction from the profile of its coefficient of friction (CoF) with time against others for 3600 seconds of operation. The observation therein suggests and confirms ample stability for F-rGO-C10 in terms of thermal stresses. Unfortunately, materials F-rGO-C6, F-rGO-C8, and F-rGO-C12 struggle to maintain stability within the operating interval of time in reducing the friction. As shown in the region marked A (0 – 750 s), F-rGO-C10 distinctly reveal reduced CoF against F-rGO-C6, F-rGO-C8 and F-rGO-C12 whose CoF falls within same limit. The attribute of F-rGO-C12 for reduced CoF falls severely within 750 – 1800 s at region marked B while F-rGO-C6 and F-rGO-C8 displays no significant activity in reduced CoF. Under these auspices, F-rGO-C10 maintains superiority attribute of stability in the reduced CoF. Surprisingly, at around 1800 – 3250 s of operation, F-rGO-C6, F-rGO-C8 and F-rGO-C12 display similar observable activity in reducing CoF less than F-rGO-C10 which still maintain its superior attribute of reduced CoF. However, within 3250 - 3600 s of operation, F-rGO- C10 still maintain appreciable and high stability for reduced CoF while F-rGO-C8 and F-rGO-C12 display no observable activity and F-rGO-C6 reveal a slight increase in CoF.

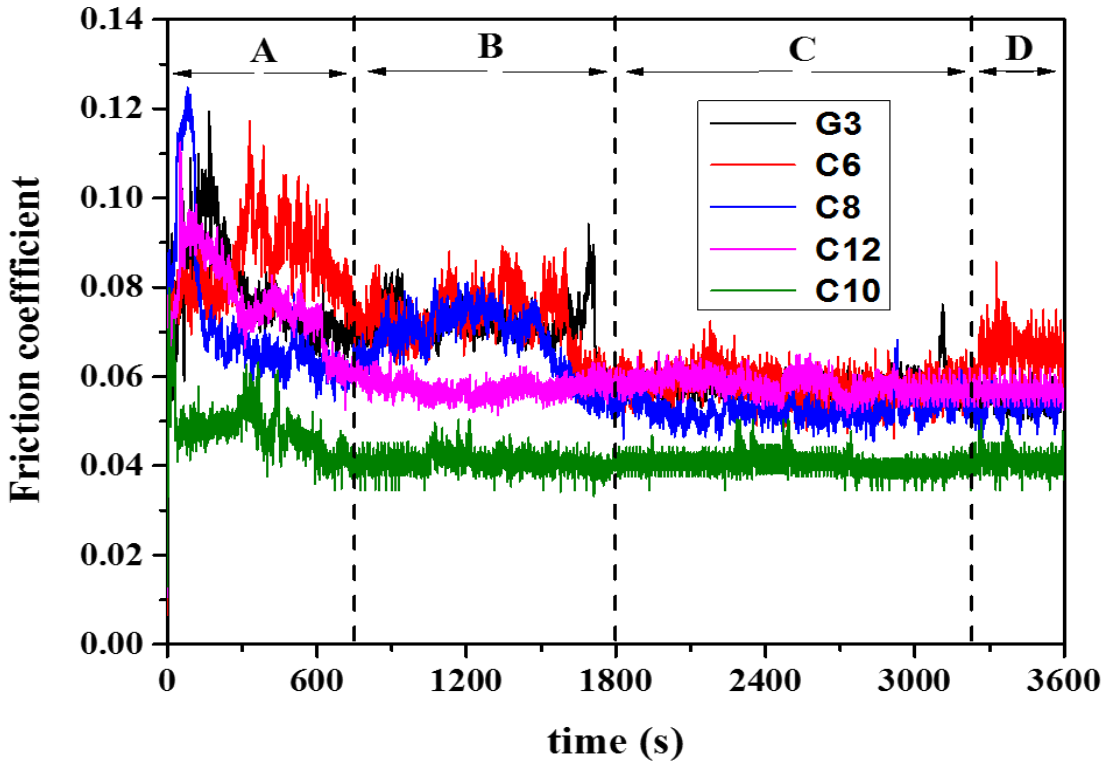

Figure 4.8: Coefficient of friction of base oil and its functionalized additives

In terms of F-rGO-C6, the coefficient of friction increases by 0.39 % compared to the base oil without additives. However, the coefficient of friction of F-rGO-C8 and F-rGO-C12 started to decrease, at 6 %. Interestingly, F-rGO-C10 shows a very large decrease in the coefficient of friction, at 36 %, which is a large leap compared to the other F-rGO samples.

4.2.2.2 Wear Scar Analysis

Similar trend can be observed in the value of specific wear rate of the same set of samples presented in Table 4.7 and Figure 4.9. Three sets for each sample were weighed before and after the four-ball test, and the values averaged. The weight losses were recorded as well.

Table 4.7: Specific wear rate of base oil and its formulated lubricant oil

Oil Sample	Initial steel ball weight (g)	Final steel ball weight (g)	Weight loss (g)
Base oil G-III	8.3570	8.3534	0.0036
G-III + FG-C6	8.3572	8.3544	0.0028
G-III + FG-C8	8.3585	8.3567	0.0018
G-III + FG-C10	8.3585	8.3573	0.0012
G-III + FG-C12	8.3580	8.3565	0.0015

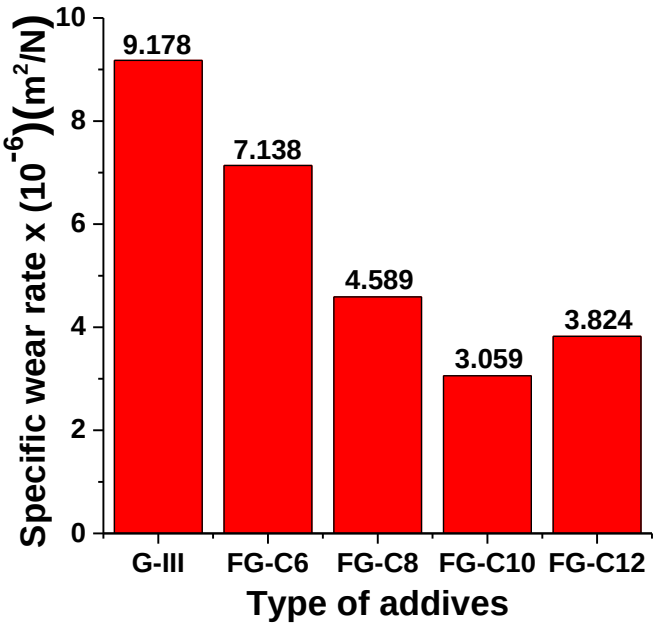

Figure 4.9: Specific wear rate of base oil and its formulated lubricant oil

It should be noted that F-rGO-C6, F-rGO-C8 and F-rGO-C10 shows similar limits. This trend can be justified by the previously mentioned trend in the degree of disorder and stretching of the bonds in the material, which decreases as the length of chain increases. This is however not applicable to F-rGO-C12, where the effect of the chain length outweighs the effect of this trend.

Four-ball tests were also performed to analyse the lubricating capabilities of the F-rGOs, which is represented by the wear of the rotating and stationary balls. To give a better picture of the wear on the balls' surfaces, the post-analysis surfaces of each steel ball was observed under SEM and the wear scar diameter (WSD) for each sample was then measured. A stable value of the friction coefficient with low variance was established through these experiments, with the value being in excellent agreement with the WSD values, as shown in Figure 4.10 and Table 4.8. All of the formulated samples decreased as the length of alkyl chain increases. However, F-rGO-C10 shows a large reduction on ball wear scar diameter data of 24 % compared to the other functionalized samples. The measurement of the wear scar diameters was obtained from the measurement of the following two diameters: the diameter along the direction of friction and the one perpendicular to the first one. This is in accordance to the standard (ISO, 2004) approved method.

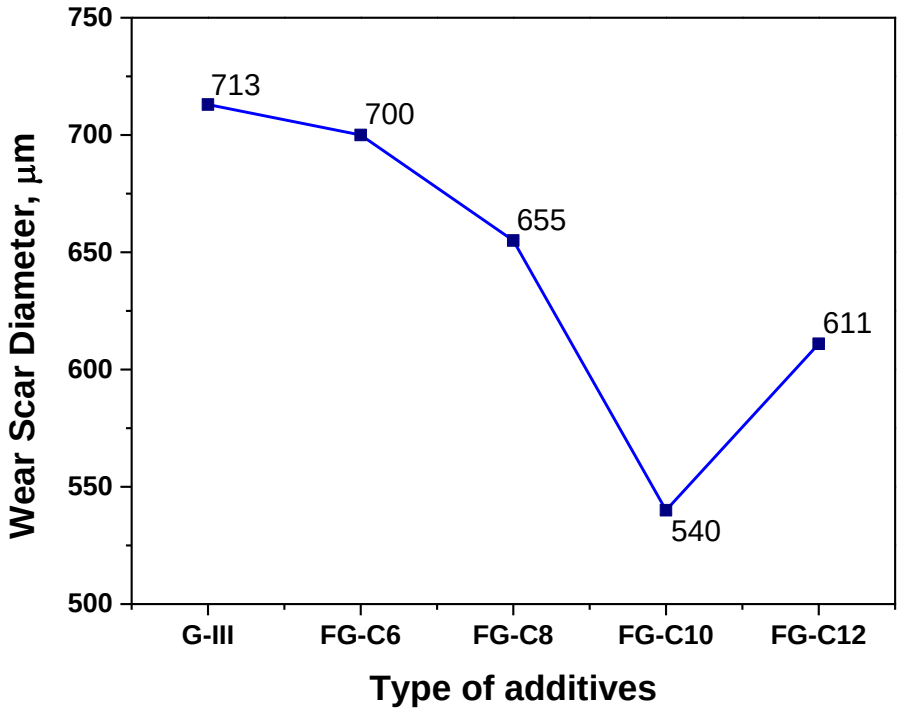

Figure 4.10: Wear scar diameter of base oil without and with additives

This can be attributed to the degree of disorder and stretching of the bonds in the F-rGO, which decreases as the length of chain increases. This is however not applicable to F-rGO-C12, where the effect of the chain length outweighs the effect of this trend. With the higher degree of order as the chain grows, the folding of the structure, as observed in the FESEM, facilitates the lowering of frictional force between the surfaces of the steel balls. This is largely due to the F-rGO in oil forming protective deposited films throughout the alkyl chains. Thus, preventing the rubbing surfaces from coming into direct contact improves the tribological behaviour of the oil. It should be pointed out that the prominent effect of the alkyl chains facilitates the formation of strong folded structures, which in turn lowers the coefficient of friction. However, there is a limit to this effect, as demonstrated by the increase in frictional force when the chain contains 12 carbon atoms.

Table 4.8: SEM images of wear scar diameter (WSD)

Sample	Wear scar diameter (µm)	Difference
Base Oil G-III	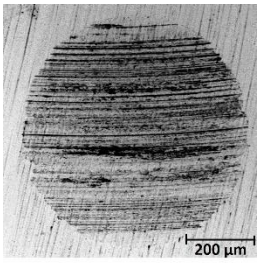 **713**	Benchmark
F-rGO-C6	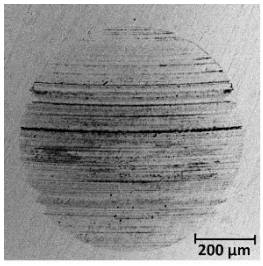 **700**	-1.8 %
F-rGO-C8	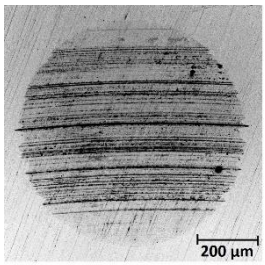 **655**	-8.1 %
F-rGO-C10	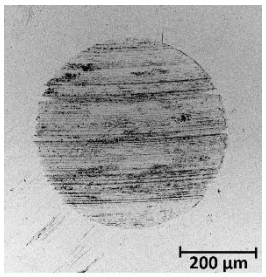 **540**	-24.3 %
F-rGO-C12	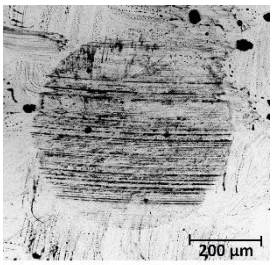 **611**	-14.3 %

All of the formulated samples decreased as the length of alkyl chain increases. However, F-rGO-C12 shows a large reduction on ball wear scar diameter data of up to 24 % compared to other functionalized samples. The results proved that functionalized rGO in oil form protective deposited films to prevent the rubbing surfaces from coming into direct contact, which improves the tribological behaviour of the oil for F-rGO-C10.

4.3 Performance of optimised additive with different concentration in lube oil

4.3.1 Physicochemical properties

4.3.1.1 Density Analysis

Table 4.9 shows the result for effect of the additive F-rGO-C10 with different concentration on the density of the oil blended at a particular temperature. The table showed that the higher the concentration of the F-rGO-C10 in the oil blend, the higher the density of oil. The test temperature for the density is 25 ºC, and the ASTM specification for the density of base oil group III falls within the range of 0.825 - 0.847 g/cm^3. The results reported in Table 4.9 conforms to this range. According to Eddy and Ekop, the average molecular weight of the oil could be tailored to the density of the oil. Therefore, the introduction of additives to the base oil can alter its molecular weight. The differential increase in the concentration of additive in the oil brought about different densities of pure base oil (Eddy & Ekop, 2007). This a significant change compared to the similar values when only the carbon chain lengths were varied. This is largely due to the higher number of particles present which accounts for the larger number of matter present in the oil. Hence, it can be said here that altering the functional group will not significantly change the density of lubricant formed as compared to the changing the concentration of additive. When the concentration of additive is kept between 0.005 to 0.05 g/cm^3 the density of the resultant lubricant oil will lie within the specified ASTM value.

Table 4.9: Density analysis of formulated lubricant oil

Oil Sample	Density (g/cm^3)
Base Oil G-III	0.843
G-III + 0.005 wt.%	0.842
G-III + 0.01 wt.%	0.843
G-III + 0.025 wt.%	0.844
G-III + 0.05 wt.%	0.845

4.3.1.2 Viscosity Analysis

As observed from Table 4.10 and Figure 4.11, both viscosity and viscosity index increased with increased concentrations of additives (Kole & Dey, 2011; Kulkarni et al., 2006; Prasher et al., 2006). The increase in the concentration of nanoparticles increases the internal shear stress of the lubricant and the viscosity.

Table 4.10: Viscosity of formulated lubricant oil

Samples	Kinematic viscosity mm^2/s	
	40 ºC	100 ºC
Base Oil G-III	33.3	6.1
G-III + 0.005 wt.%	35.3	6.5
G-III + 0.01 wt.%	36.5	6.7
G-III + 0.025 wt.%	37.9	7.0
G-III + 0.05 wt.%	39.1	7.3

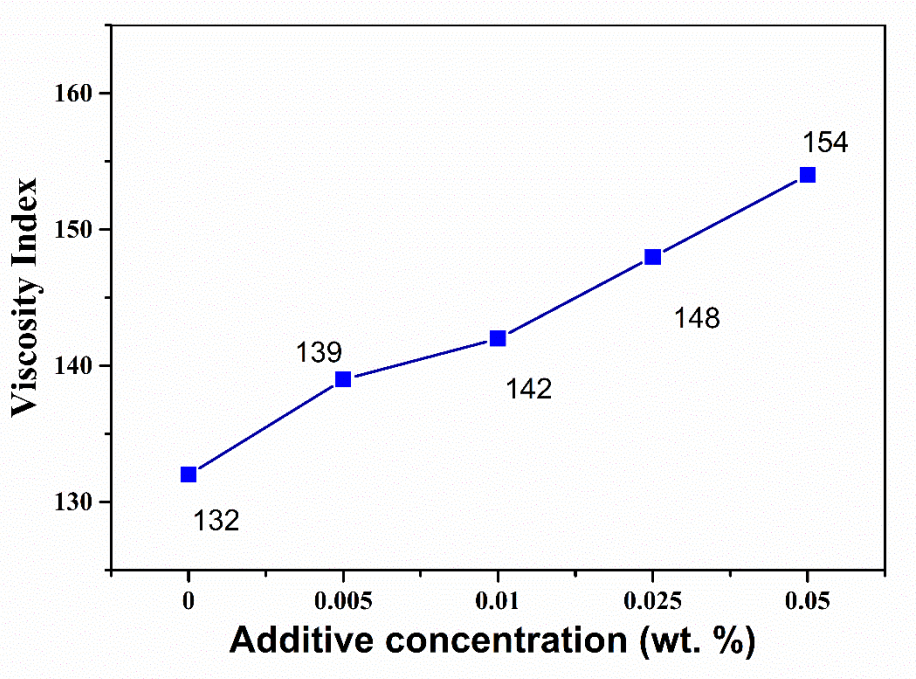

Figure 4.11: VI of base oil and F-rGO-C10 additives with different concentration

The weakening of inter-particle and inter molecular adhesion forces are the driving forces behind this observation (Kulkarni et al., 2006). This is also attributed to the previously mentioned effect of increasing molecular weight which lead to higher stability towards temperature (Ghosh et al., 2011). The viscosity and viscosity index of the F-rGO-C10 with 0.050 wt. % nanoparticles based lubricant were found to be higher than pure base oil and other functionalized additives. Thus, 0.050 wt. % of F-rGO-C10 would have a better film forming tendency at higher temperatures compared to 0.005, 0.010 and 0.025 wt. %.

4.3.1.3 Total acid number Analysis

The data of the TAN are shown in Table 4.11. The data showed that the pure base oil has no resistance to oxidation, but increasing the concentration of additives pass 0.010 wt. % resulted in increase of the total acid numbers. Interaction of the carbon component of the additive and oxygen from surrounding lead to formation of carbonyl compounds which further oxidises especially in the presence of heat to form carboxylic acids (Fox et al., 1991). This chain of event lead to the observed increase in the total acid number of

the base oil. From the data in the table, it can be observed that past 0.010 wt. % of additive added lead to significant increase to TAN, higher even than the base oil without any additive added to it. At elevated temperature, the effect of this phenomenon is much more prominent such that the formed carbonyl and carboxylic containing compounds may polymerize leading to sludge being precipitated, thus increasing the wear (Fox et al., 1991). Therefore, it is paramount to use 0.010 wt. % of additive as the threshold for the amount to be added to the base oil to increase its lubricant properties without having detrimental effect on the base oil, in this case increasing its corrosive property.

Table 4.11: TAN of base oil without additive and with different concentration of additives

Samples	TAN (mg KOH/g)	
	Before four-ball test	**After four-ball test**
Base oil G-III	0.07	0.11
G-III + 0.005 wt.%	0.07	0.12
G-III + 0.010 wt.%	0.06	0.08
G-III + 0.025 wt.%	0.12	0.25
G-III + 0.050 wt.%	0.32	0.48

4.3.2 Tribological study

4.3.2.1 Friction coefficient

F-rGO-C10 was selected as the best additive. As observed from Figure 4.12, the coefficient of friction at different concentrations of F-rGO-C10 decreases as the concentration decreases. The trend follows in the order 0.050 wt. % and 0.025 wt. %, while 0.005 wt. % shows a slightly higher coefficient of friction than 0.010 wt. %. This observation is very much due to the increment of particle in the oil present as the concentration increases. As pointed out previously this increment lead to increasing density, viscosity and acid number. The latter value in particular lead to corrosion in between the surfaces, a phenomenon which is even more prominent at higher temperatures. Thus 0.010 wt. % of additive is the threshold after which the coefficient will increase due to prominent decrease in the efficiency of the lubricant.

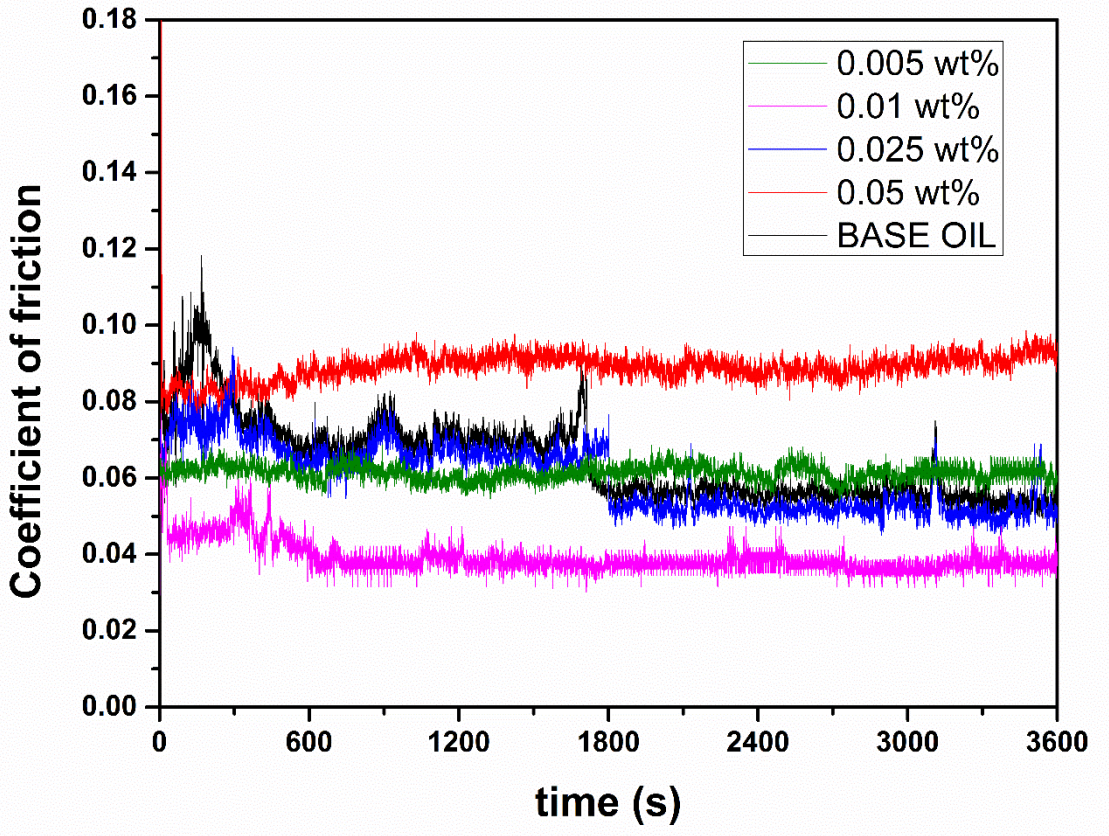

Figure 4.12: Comparison of CoF with different concentration of F-rGO-C10

4.3.2.2 Wear Scar Analysis

Table 4.12 shows the value of specific wear rates of the same set of F-rGO-C10 at different concentrations. There is a steady drop in the specific wear rate value of up to 67 % (0.010 wt. %). Although there are only 36 % and 6 % drop in the value for 0.005 wt. % and 0.025 wt. %, these values are still considerably low when compared to pure oil. These observations corroborate the observations on the increasing coefficient of friction and further lend support to the postulation that 0.010 wt. % is the threshold value for the efficiency of the lubrication.

Table 4.12: Specific wear rate of F-rGO-C10 with different concentration

Additive concentration (wt. %)	Initial steel ball weight (g)	Final steel ball weight (g)	Weight loss (g)
Base Oil G-III	8.3570	8.3534	0.0036
0.005	8.3578	8.3555	0.0023
0.010	8.3585	8.3573	0.0012
0.025	8.3602	8.3568	0.0034
0.050	8.3624	8.3585	0.0039

The results for both friction and wear analysis this time around indicates that approximately 0.010 wt. % of additives yield the best lubrication effect. This is very much due to overall better characteristic of the lubricant oil yielded from this particular concentration specifically its density, viscosity and acid number. The density and viscosity of the oil allows for proper lubrication boundary between the steel surfaces while the stability of the oil towards oxidation prevents corrosion due to acidity to take place on the surfaces involved.

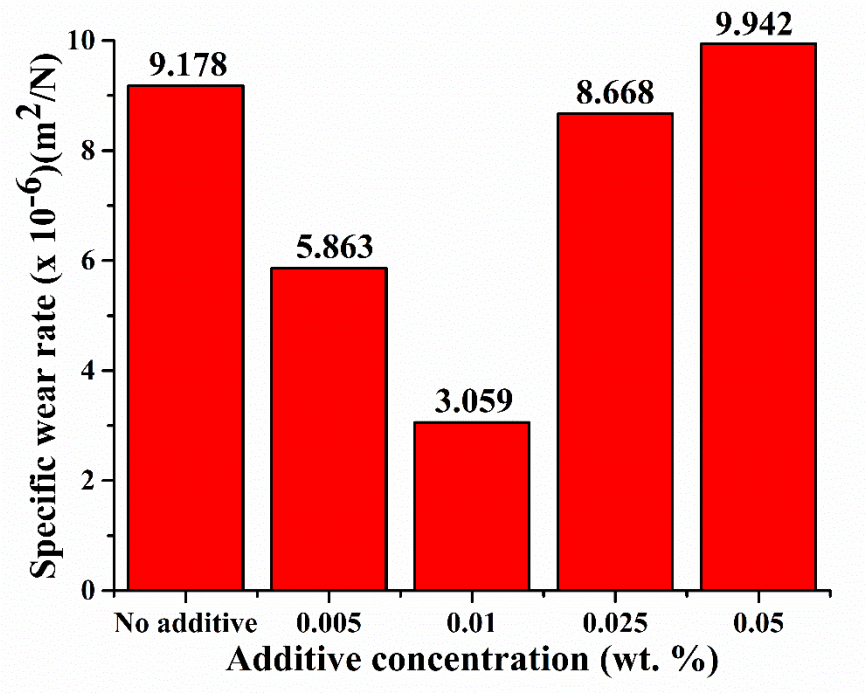

Figure 4.13: Specific wear rate of lubricant oil with different additive concentration

CHAPTER 5: CONCLUSION AND RECOMMENDATION

5.1 Conclusion

This study was successful in synthesizing F-rGO, which was then applied as an additive in base oil. Table 5.1 below is a summary of the advancement in tribological field as a result of this research in terms of the tribological properties and its applicability in the field.

Table 5.1: Comparison of recent solid additives with present research on their tribological properties

Solid additive	Concentration of additive (wt. %)	Liquid base	Wear reduction (%)	CoF reduction (%)	Reference
MWCNTs	0.10	PAO	16	14	(Y. Peng et al., 2007)
MoS_2	0.5	Liquid Paraffin	7	54	(Hu et al., 2009)
GO	0.10	SN 150	30	16	(Senatore et al., 2013)
h-BN	1.0	water	7	15	(Cho et al., 2013)
F-rGO	0.01	Base oil G-III	24	36	In this work

The following can be concluded from the present work:

- The antiwear properties of base oils were enhanced by using synthesized functionalized rGO.
- There was a reduction in both the coefficient of friction (36 %) and wear (24 %) in the case of 0.01 wt. % F-rGO-C10 compared with the base oil and other F-rGOs.

- The coefficient of friction in the case of 0.010 wt. % additive was lesser than pure base oil and base oil containing 0.005 wt. %, 0.025 wt. %, and 0.050 wt. %.
- The viscosity index increased as concentrations of additives increase. 0.050 wt. % of F-rGO-C10 reported higher viscosity index compared to 0.025 wt. %, 0.010 wt. %, and 0.005 wt. %.
- In comparison with base oil, all synthesized additive showed better TAN, as the TAN value is less than 0.01 mg KOH/g.
- Mechanisms such as rolling, mending, and protective layer formation of nanoparticles between the mating surfaces could be responsible for reducing the specific wear rate and CoF.
- As observed from the SEM images, the WSD of steel ball surfaces were decreasing with increasing alkyl functionality compared to mineral oil.
- As observed from this work, a minimum of 0.010 wt. % F-rGO-C10 were required to enhance the antiwear properties of the lubricant.

5.2 Recommendations for future work

This research could be extended into many practical applications of functionalized reduced graphene oxide in tribological industries:

- Feasibility study on different temperature and different load to study the extreme pressure additive used under heavier loads at high temperatures.
- Formulate lubricants with various concentration of additives to study the optimisation of lube oil.
- Formulate the lubricant with different types of base oil to study the compatibility of functionalized rGO with different base oil.
- Other types of mechanical characterisation for tribology, such as High Frequency Reciprocating Rig (HFRR), ball-on-disc, and pin-on-disc can be carried out to elucidate the performance of the additive.
- Study on separating the lubricant oil from the additives to improve the reusability of the oil. The separation can be done via single or composite solvent extraction and acid treatment.

REFERENCES

Ahlquist, M., & Fokin, V. V. (2007). Enhanced reactivity of dinuclear copper (I) acetylides in dipolar cycloadditions. *Organometallics, 26*(18), 4389-4391.

ASTM, A. (2013). Standard Terminology Relating to Wear and Erosion. *G40*.

Bautista, C., & Mendoza, D. (2011). Multilayer graphene synthesized by CVD using liquid hexane as the carbon precursor. *arXiv preprint arXiv:1109.1318*.

Berman, D., Erdemir, A., & Sumant, A. V. (2013). Few layer graphene to reduce wear and friction on sliding steel surfaces. *Carbon, 54*, 454-459.

Berman, D., Erdemir, A., & Sumant, A. V. (2014). Graphene: a new emerging lubricant. *Materials Today, 17*(1), 31-42.

Berman, D., Erdemir, A., Zinovev, A. V., & Sumant, A. V. (2015). Nanoscale friction properties of graphene and graphene oxide. *Diamond and Related Materials, 54*, 91-96.

Bock, V. D., Hiemstra, H., & Van Maarseveen, J. H. (2006). CuI-Catalyzed Alkyne–Azide "Click" Cycloadditions from a Mechanistic and Synthetic Perspective. *European Journal of Organic Chemistry, 2006*(1), 51-68.

Boshui, C., Junxiu, D., & Guoxu, C. (1996). Tribochemistry of gadolinium dialkyldithiophosphate. *Wear, 196*(1-2), 16-20.

Brodie, B. C. (1859). On the atomic weight of graphite. *Philosophical Transactions of the Royal Society of London, 149*, 249-259.

Bruker. (2016). D8 ADVANCE. Retrieved 17 February, 2017, from https://www.bruker.com/products/x-ray-diffraction-and-elemental-analysis/x-ray-diffraction/d8-advance/overview.html

Cai, D., & Song, M. (2007). Preparation of fully exfoliated graphite oxide nanoplatelets in organic solvents. *Journal of Materials Chemistry, 17*(35), 3678-3680.

Carotenuto, G., Longo, A., Nicolais, L., De Nicola, S., Pugliese, E., Ciofini, M., Locatelli, M., Lapucci, A., & Meucci, R. (2015). Laser-Induced Thermal Expansion of H2SO4-Intercalated Graphite Lattice. *The Journal of Physical Chemistry C, 119*(28), 15942-15947.

Charlier, J.-C., Gonze, X., & Michenaud, J.-P. (1994). First-principles study of the stacking effect on the electronic properties of graphite (s). *Carbon, 32*(2), 289-299.

Chen, W., Yan, L., & Bangal, P. R. (2010). Preparation of graphene by the rapid and mild thermal reduction of graphene oxide induced by microwaves. *Carbon, 48*(4), 1146-1152.

Cho, D.-H., Kim, J.-S., Kwon, S.-H., Lee, C., & Lee, Y.-Z. (2013). Evaluation of hexagonal boron nitride nano-sheets as a lubricant additive in water. *Wear, 302*(1), 981-986.

Choi, E.-Y., Han, T. H., Hong, J., Kim, J. E., Lee, S. H., Kim, H. W., & Kim, S. O. (2010). Noncovalent functionalization of graphene with end-functional polymers. *Journal of Materials Chemistry, 20*(10), 1907-1912.

Deetuam, C., Samthong, C., Thongyai, S., Praserthdam, P., & Somwangthanaroj, A. (2014). Synthesis of well dispersed graphene in conjugated poly (3, 4-ethylenedioxythiophene): polystyrene sulfonate via click chemistry. *Composites Science and Technology, 93*, 1-8.

Eddy, N., & Ekop, A. (2007). Effect of additives on some physical parameters of palm oil. *Journal of Chemistry, 4*(3), 350-353.

Elmer, P. (2017). Spotlight 400 FT-IR Imaging System. Retrieved 17 February, 2017, from http://www.perkinelmer.com/searchresult?searchName=ftir&_csrf=fe347778-c5f3-41dc-b2a5-7626cdafeca1

Espinosa, T., Sanes, J., & Bermúdez, M.-D. (2016). New Alkylether–Thiazolium Room-Temperature Ionic Liquid Lubricants: Surface Interactions and Tribological Performance. *ACS Applied Materials & Interfaces, 8*(28), 18631-18639. doi: 10.1021/acsami.6b05888

Fajardo, O. Y., Bresme, F., Kornyshev, A. A., & Urbakh, M. (2015). Electrotunable Friction with Ionic Liquid Lubricants: How Important Is the Molecular Structure of the Ions? *The Journal of Physical Chemistry Letters, 6*(20), 3998-4004. doi: 10.1021/acs.jpclett.5b01802

Fox, M., Pawlak, Z., & Picken, D. (1991). Acid-base determination of lubricating oils. *Tribology International, 24*(6), 335-340.

Franc, G., & Kakkar, A. (2008). Dendrimer design using Cu I-catalyzed alkyne–azide "click-chemistry". *Chemical Communications*(42), 5267-5276.

Georgakilas, V., Otyepka, M., Bourlinos, A. B., Chandra, V., Kim, N., Kemp, K. C., Hobza, P., Zboril, R., & Kim, K. S. (2012). Functionalization of graphene: covalent and non-covalent approaches, derivatives and applications. *Chemical reviews, 112*(11), 6156-6214.

Ghosh, P., Das, T., & Nandi, D. (2011). Shear stability and thickening properties of homo and copolymer of methyl methacrylate. *American Journal of Polymer Science, 1*(1), 1-5.

Godfrey, D. (1965). The lubrication mechanism of tricresyl phosphate on steel. *ASLE TRANSACTIONS, 8*(1), 1-11.

Golas, P. L., & Matyjaszewski, K. (2010). Marrying click chemistry with polymerization: expanding the scope of polymeric materials. *Chemical Society Reviews, 39*(4), 1338-1354.

Han, N. R., & Cho, J. W. (2016). Click coupled stitched graphene sheets and their polymer nanocomposites with enhanced photothermal and mechanical properties. *Composites Part A: Applied Science and Manufacturing, 87*, 78-85.

Handbook, A., & Friction, L. (1992). Wear Technology, vol. 18. *ASM International, USA*, 1482.

Hein, J. E., & Fokin, V. V. (2010). Copper-catalyzed azide–alkyne cycloaddition (CuAAC) and beyond: new reactivity of copper (I) acetylides. *Chemical Society Reviews, 39*(4), 1302-1315.

Himo, F., Lovell, T., Hilgraf, R., Rostovtsev, V. V., Noodleman, L., Sharpless, K. B., & Fokin, V. V. (2005). Copper (I)-catalyzed synthesis of azoles. DFT study predicts unprecedented reactivity and intermediates. *Journal of the American Chemical Society, 127*(1), 210-216.

Hu, K., Liu, M., Wang, Q., Xu, Y., Schraube, S., & Hu, X. (2009). Tribological properties of molybdenum disulfide nanosheets by monolayer restacking process as additive in liquid paraffin. *Tribology International, 42*(1), 33-39.

Huang, H., Tu, J., Zou, T., Zhang, L., & He, D. (2005). Friction and wear properties of IF–MoS2 as additive in paraffin oil. *Tribology letters, 20*(3-4), 247-250.

Huisgen, R. (1963). 1, 3-dipolar cycloadditions. Past and future. *Angewandte Chemie International Edition in English, 2*(10), 565-598.

Hummers Jr, W. S., & Offeman, R. E. (1958). Preparation of graphitic oxide. *Journal of the American Chemical Society, 80*(6), 1339-1339.

Iha, R. K., Wooley, K. L., Nystrom, A. M., Burke, D. J., Kade, M. J., & Hawker, C. J. (2009). Applications of orthogonal "click" chemistries in the synthesis of functional soft materials. *Chemical reviews, 109*(11), 5620-5686.

Instruments, D. (2017). Four Ball Tester. Retrieved 17 February, 2017, from http://ducom.com/test-instruments/lubricant-testers/four-ball-tester/

ISO, S. (2004). 20623: 2004: Petroleum and related products-Determination of the extreme-pressure and anti-wear properties of fluids—Four ball method: European conditions)(20623: 2003).

Jang, J., Pham, V. H., Hur, S. H., & Chung, J. S. (2014). Dispersibility of reduced alkylamine-functionalized graphene oxides in organic solvents. *Journal of colloid and interface science, 424*, 62-66.

Javed, S. I., & Hussain, Z. (2015). Covalently Functionalized Graphene Oxide–Characterization and Its Electrochemical Performance. *International Journal of Electrochemical Science, 10*, 9475-9487.

Javidialesaadi, A., & Raeissi, S. (2013). Biodiesel production from high free fatty acid-content oils: experimental investigation of the pretreatment step. *APCBEE Procedia, 5*, 474-478.

Jianqiang, H., Huanqin, Z., Li, W., Xianyong, W., Feng, J., & Zhiming, Z. (2005). Study on tribological properties and action mechanism of organic cadmium compound in lubricants. *Wear, 259*(1), 519-523.

Kasrai, M., Cutler, J., Gore, K., Canning, G., Bancroft, G., & Tan, K. (1998). The chemistry of antiwear films generated by the combination of ZDDP and MoDTC examined by X-ray absorption spectroscopy. *Tribology transactions, 41*(1), 69-77.

Kato, K. (1992). Micro-mechanisms of wear—wear modes. *Wear, 153*(1), 277-295.

Khruschov, M. (1974). Principles of abrasive wear. *Wear, 28*(1), 69-88.

Kimura, Y., Wakabayashi, T., Okada, K., Wada, T., & Nishikawa, H. (1999). Boron nitride as a lubricant additive. *Wear, 232*(2), 199-206.

Kolb, H. C., Finn, M., & Sharpless, K. B. (2001). Click chemistry: diverse chemical function from a few good reactions. *Angewandte Chemie International Edition, 40*(11), 2004-2021.

Kole, M., & Dey, T. (2011). Effect of aggregation on the viscosity of copper oxide–gear oil nanofluids. *International Journal of Thermal Sciences, 50*(9), 1741-1747.

Kou, L., He, H., & Gao, C. (2010). Click chemistry approach to functionalize two-dimensional macromolecules of graphene oxide nanosheets. *Nano-Micro Letters, 2*(3), 177-183.

Kulkarni, D. P., Das, D. K., & Chukwu, G. A. (2006). Temperature dependent rheological property of copper oxide nanoparticles suspension (nanofluid). *Journal of nanoscience and nanotechnology, 6*(4), 1150-1154.

Li, J., Peng, Q., Bai, G., & Jiang, W. (2005). Carbon scrolls produced by high energy ball milling of graphite. *Carbon, 43*(13), 2830-2833.

Liang, L., & Astruc, D. (2011). The copper (I)-catalyzed alkyne-azide cycloaddition (CuAAC)"click" reaction and its applications. An overview. *Coordination Chemistry Reviews, 255*(23), 2933-2945.

Lin, J., Wang, L., & Chen, G. (2011). Modification of graphene platelets and their tribological properties as a lubricant additive. *Tribology Letters, 41*(1), 209-215.

Lu, R., Kobayashi, K., Nanao, H., & Mori, S. (2009). Deactivation effect of tricresyl phosphate (TCP) on tribochemical decomposition of hydrocarbon oil on a nascent steel surface. *Tribology letters, 33*(1), 1-8.

Lutz, J.-F., & Börner, H. G. (2008). Modern trends in polymer bioconjugates design. *Progress in Polymer Science, 33*(1), 1-39.

Lutz, J.-F., & Zarafshani, Z. (2008). Efficient construction of therapeutics, bioconjugates, biomaterials and bioactive surfaces using azide–alkyne "click" chemistry. *Advanced drug delivery reviews, 60*(9), 958-970.

Mansfeld, U., Pietsch, C., Hoogenboom, R., Becer, C. R., & Schubert, U. S. (2010). Clickable initiators, monomers and polymers in controlled radical polymerizations–a prospective combination in polymer science. *Polymer Chemistry*, *1*(10), 1560-1598.

Marcano, D. C., Kosynkin, D. V., Berlin, J. M., Sinitskii, A., Sun, Z., Slesarev, A., Alemany, L. B., Lu, W., & Tour, J. M. (2010). Improved synthesis of graphene oxide. *ACS nano*, *4*(8), 4806-4814.

Marques, P., Sousa, A., Gonçalves, G., Grácio, J., Singh, M., Almeida, N., & Cruz, S. (2011). *Functionalized graphene nanocomposites*: INTECH Open Access Publisher.

Meldal, M., & Tornøe, C. W. (2008). Cu-catalyzed azide− alkyne cycloaddition. *Chemical reviews*, *108*(8), 2952-3015.

Metrohm. (2017). Titration. Retrieved 15 February, 2017, from https://www.metrohm.com/en/products/titration/?gclid=Cj0KEQiAuJXFBRDirIGnpZLE-N4BEiQAqV0KGgED42lj-9RzxtfDc0wleuT-g_84se1yD36pR_EsIZIaAoNn8P8HAQ

Mullen, D. G., McNerny, D. Q., Desai, A., Cheng, X.-m., DiMaggio, S. C., Kotlyar, A., Zhong, Y., Qin, S., Kelly, C. V., & Thomas, T. P. (2011). Design, synthesis, and biological functionality of a dendrimer-based modular drug delivery platform. *Bioconjugate chemistry*, *22*(4), 679-689.

Mungse, H. P., Kumar, N., & Khatri, O. P. (2015). Synthesis, dispersion and lubrication potential of basal plane functionalized alkylated graphene nanosheets. *RSC Advances*, *5*(32), 25565-25571.

Nia, A. S., Rana, S., Döhler, D., Noirfalise, X., Belfiore, A., & Binder, W. H. (2014). Click chemistry promoted by graphene supported copper nanomaterials. *Chemical Communications*, *50*(97), 15374-15377.

Novoselov, K., & Geim, A. (2007). The rise of graphene. *Nature Materials*, *6*, 183-191.

Paar, A. (2017). Stabinger Viscometer™ Series. Retrieved 16 January, 2017, from http://www.anton-paar.com/corp-en/products/details/svmTM-series/

Pan, Y., Bao, H., Sahoo, N. G., Wu, T., & Li, L. (2011). Water-soluble poly (N-isopropylacrylamide)–graphene sheets synthesized via click chemistry for drug delivery. *Advanced Functional Materials*, *21*(14), 2754-2763.

Peng, D., Kang, Y., Hwang, R., Shyr, S., & Chang, Y. (2009). Tribological properties of diamond and SiO 2 nanoparticles added in paraffin. *Tribology International*, *42*(6), 911-917.

Peng, Y., Hu, Y., & Wang, H. (2007). Tribological behaviors of surfactant-functionalized carbon nanotubes as lubricant additive in water. *Tribology Letters*, *25*(3), 247-253.

Prasher, R., Phelan, P. E., & Bhattacharya, P. (2006). Effect of aggregation kinetics on the thermal conductivity of nanoscale colloidal solutions (nanofluid). *Nano letters, 6*(7), 1529-1534.

Rabinowicz, E. (1965). Friction and wear of materials.

Raghunanan, L., & Narine, S. S. (2016a). Engineering Green Lubricants I: Optimizing Thermal and Flow Properties of Linear Diesters Derived from Vegetable Oils. *ACS Sustainable Chemistry & Engineering, 4*(3), 686-692. doi: 10.1021/acssuschemeng.5b01644

Raghunanan, L., & Narine, S. S. (2016b). Engineering Green Lubricants II: Thermal Transition and Flow Properties of Vegetable Oil-Derived Diesters. *ACS Sustainable Chemistry & Engineering, 4*(3), 693-700. doi: 10.1021/acssuschemeng.5b01708

Raghunanan, L., & Narine, S. S. (2016c). Engineering Green Lubricants IV: Influence of Structure on the Thermal Behavior of Linear and Branched Aliphatic Fatty Acid-Derived Diesters. *ACS Sustainable Chemistry & Engineering, 4*(9), 4868-4874. doi: 10.1021/acssuschemeng.6b01144

Ramasamy, M. S., Mahapatra, S. S., & Cho, J. W. (2015). Functionalization of graphene with self-doped conducting polypyrrole by click coupling. *Journal of colloid and interface science, 455*, 63-70.

Rasheed, A., Khalid, M., Rashmi, W., Gupta, T., & Chan, A. (2016). Graphene based nanofluids and nanolubricants–Review of recent developments. *Renewable and Sustainable Energy Reviews, 63*, 346-362.

Rasheed, A. K., Khalid, M., Walvekar, R., Gupta, T. C. S. M., & Chan, A. (2015). Study of graphene nanolubricant using thermogravimetric analysis. *Journal of Materials Research*, 1-8.

Renishaw. (2017). inVia™ confocal Raman microscope. Retrieved 16 January, 2017, from http://www.renishaw.com/en/invia-confocal-raman-microscope--6260

Rodionov, V. O., Presolski, S. I., Díaz Díaz, D., Fokin, V. V., & Finn, M. (2007). Ligand-accelerated Cu-catalyzed azide− alkyne cycloaddition: A mechanistic report. *Journal of the American Chemical Society, 129*(42), 12705-12712.

Rostovtsev, V. V., Green, L. G., Fokin, V. V., & Sharpless, K. B. (2002). A stepwise huisgen cycloaddition process: copper (I)-catalyzed regioselective "ligation" of azides and terminal alkynes. *Angewandte Chemie, 114*(14), 2708-2711.

Rudnick, L. R. (2009). *Lubricant additives: chemistry and applications*: CRC press.

Sakamoto, T., Uetz, H., & Föhl, J. (1985). Reaction layer formation on bronze with an SP extreme pressure additive in boundary lubrication under increasing load: I. *Wear, 105*(4), 307-321.

Salvio, R., Krabbenborg, S., Naber, W. J., Velders, A. H., Reinhoudt, D. N., & van der Wiel, W. G. (2009). The Formation of Large-Area Conducting Graphene-Like Platelets. *Chemistry–A European Journal, 15*(33), 8235-8240.

Scientific, T. F. (2016). Scanning Electron Microscope. Retrieved 28 December, 2016, from https://www.fei.com/products/sem/quanta-sem/

Senatore, A., D'Agostino, V., Petrone, V., Ciambelli, P., & Sarno, M. (2013). Graphene Oxide Nanosheets as Effective Friction Modifier for Oil Lubricant: Materials, Methods, and Tribological Results. *ISRN Tribology, 2013*.

Shankara, A., Menezes, P. L., Simha, K., & Kailas, S. V. (2008). Study of solid lubrication with MoS2 coating in the presence of additives using reciprocating ball-on-flat scratch tester. *Sadhana, 33*(3), 207-220.

Sharma, B. K., Adhvaryu, A., Sahoo, S. K., Stipanovic, A. J., & Erhan, S. Z. (2004). Influence of chemical structures on low-temperature rheology, oxidative stability, and physical properties of group II and III base oils. *Energy & fuels, 18*(4), 952-959.

Shioyama, H., & Akita, T. (2003). A new route to carbon nanotubes. *Carbon, 41*(1), 179-181.

Straub, B. F. (2007). μ-Acetylide and μ-alkenylidene ligands in "click" triazole syntheses. *Chemical Communications*(37), 3868-3870.

Suarez, A. N., Grahn, M., Pasaribu, R., & Larsson, R. (2010). The influence of base oil polarity on the tribological performance of zinc dialkyl dithiophospate additives. *Tribology International, 43*(12), 2268-2278.

Suh, N. P. (1973). The delamination theory of wear. *Wear, 25*(1), 111-124.

Sumerlin, B. S., & Vogt, A. P. (2009). Macromolecular engineering through click chemistry and other efficient transformations. *Macromolecules, 43*(1), 1-13.

Sun, S., Cao, Y., Feng, J., & Wu, P. (2010). Click chemistry as a route for the immobilization of well-defined polystyrene onto graphene sheets. *Journal of Materials Chemistry, 20*(27), 5605-5607.

Sunqing, Q., Junxiu, D., & Guoxu, C. (1999). A review of ultrafine particles as antiwear additives and friction modifiers in lubricating oils. *Lubrication Science, 11*(3), 217-226.

Tantis, I., Psarras, G., & Tasis, D. (2012). Functionalized graphene–poly (vinyl alcohol) nanocomposites: physical and dielectric properties. *Express Polym Lett, 6*(4), 283-292.

Toledo, M. (2016). Thermogravimetric Analysis (TGA). Retrieved 28 December, 2016, from http://www.mt.com/gb/en/home/products/Laboratory_Analytics_Browse/TA_Family_Browse/TGA.html

Tornøe, C. W., Christensen, C., & Meldal, M. (2002). Peptidotriazoles on solid phase:[1, 2, 3]-triazoles by regiospecific copper (I)-catalyzed 1, 3-dipolar cycloadditions of terminal alkynes to azides. *The Journal of organic chemistry, 67*(9), 3057-3064.

ULVAC-PHI, I. (2017). X-ray Photoelectron Spectroscopy / XPS. Retrieved 18 January, 2017, from https://www.ulvac-phi.com/en/products/xps/phi-quantera-ii/

Unnikrishnan, R., Jain, M., Harinarayan, A., & Mehta, A. (2002). Additive–additive interaction: an XPS study of the effect of ZDDP on the AW/EP characteristics of molybdenum based additives. *Wear, 252*(3), 240-249.

Wang, H.-X., Zhou, K.-G., Xie, Y.-L., Zeng, J., Chai, N.-N., Li, J., & Zhang, H.-L. (2011). Photoactive graphene sheets prepared by "click" chemistry. *Chemical Communications, 47*(20), 5747-5749.

Wang, L.-F., Ma, T.-B., Hu, Y.-Z., & Wang, H. (2012). Atomic-scale friction in graphene oxide: an interfacial interaction perspective from first-principles calculations. *Physical Review B, 86*(12), 125436.

Xia, Z., Leonardi, F., Gobbi, M., Liu, Y., Bellani, V., Liscio, A., Kovtun, A., Li, R., Feng, X., & Orgiu, E. (2016). Electrochemical Functionalization of Graphene at the Nanoscale with Self-Assembling Diazonium Salts. *ACS nano, 10*(7), 7125-7134.

Xiaodong, Z., Xun, F., Huaqiang, S., & Zhengshui, H. (2007). Lubricating properties of Cyanex 302-modified MoS2 microspheres in base oil 500SN. *Lubrication Science, 19*(1), 71-79.

Xu, C., Wang, X., & Zhu, J. (2008). Graphene− metal particle nanocomposites. *The Journal of Physical Chemistry C, 112*(50), 19841-19845.

Xu, J., Kato, K., & Hirayama, T. (1997). The transition of wear mode during the running-in process of silicon nitride sliding in water. *Wear, 205*(1), 55-63.

Ye, Y.-S., Chen, Y.-N., Wang, J.-S., Rick, J., Huang, Y.-J., Chang, F.-C., & Hwang, B.-J. (2012). Versatile grafting approaches to functionalizing individually dispersed graphene nanosheets using RAFT polymerization and click chemistry. *Chemistry of Materials, 24*(15), 2987-2997.

Zhang, D.-D., Zu, S.-Z., & Han, B.-H. (2009). Inorganic–organic hybrid porous materials based on graphite oxide sheets. *Carbon, 47*(13), 2993-3000.

Zhang, J., Liu, W., Xue, Q., & Wang, Q. (1998). Investigation of the friction and wear behaviors of Cu (I) and Cu (II) dioctyldithiophosphates as additives in liquid paraffin. *Wear, 216*(1), 35-40.

Zhang, L., Chen, X., Xue, P., Sun, H. H., Williams, I. D., Sharpless, K. B., Fokin, V. V., & Jia, G. (2005). Ruthenium-catalyzed cycloaddition of alkynes and organic azides. *Journal of the American Chemical Society, 127*(46), 15998-15999.

Zhou, Y., Bao, Q., Tang, L. A. L., Zhong, Y., & Loh, K. P. (2009). Hydrothermal dehydration for the "green" reduction of exfoliated graphene oxide to graphene

and demonstration of tunable optical limiting properties. *Chemistry of Materials, 21*(13), 2950-2956.

Zou, Y., & Wang, Y. (2011). NiO nanosheets grown on graphene nanosheets as superior anode materials for Li-ion batteries. *Nanoscale, 3*(6), 2615-2620.

LIST OF PUBLICATIONS AND PAPERS PRESENTED

Nadia Jamal, Samira Bagheri, Sharifah Bee Abd Hamid. (2016). Chemical functionalization of graphene for lubricant oil. The 1st UKM-ISESCO-COMSATS International Workshop on Nanotechnology for Young Scientists (IWYS2016)

Jamal, N., Bagheri, S., Abd Hamid, S. B. Antiwear additive via click chemistry: Probing effect of alkyl chain length, ID: LS-16-0147-RA-LS (UNDER REVIEW)

APPENDIX

Table A-1: CoF value of 0.010 wt. % additives added in base oil

Sample, wt. %	Load (N)	Time (second)	Maximum	Minimum	Mean	Standard Deviation ($x10^{-3}$)
Base oil G-III	400	3600	0.119	0.014	0.066	10.683
FrGO-C6	400	3600	0.117	0.007	0.069	11.849
FrGO-C8	400	3600	0.125	0.019	0.061	11.794
FrGO-C10	400	3600	0.080	0.013	0.042	4.204
FrGO-C12	400	3600	0.112	0.011	0.062	8.979

Table A-2: CoF value for F-rGO-C10 added in base oil with concentration varies from 0.005 wt. % - 0.050 wt. %

FrGO-C10 (wt. %)	Load (N)	Time (second)	Maximum	Minimum	Mean	Standard Deviation ($x10^{-3}$)
0.000	400	3600	0.119	0.014	0.066	10.683
0.005	400	3600	0.070	0.051	0.058	2.065
0.010	400	3600	0.080	0.013	0.042	4.204
0.025	400	3600	0.100	0.050	0.066	8.802
0.050	400	3600	0.216	0.014	0.096	4.059